Revealing protein vibrational modes using plasmonic surfaces

Sharif Zaidouni

Bachelor Assignment report
Biomedical Technology

Daily supervisor: M.R. Aghdaee (MohammadReza)
Main supervisor: dr. O.S. Ojambati (Femi)
External member: dr. S. Pudd (Sergii)

Dynamic NanoPhotonics,
NanoBioPhysics
Faculty of Science and Technology

July 10, 2023

UNIVERSITY OF TWENTE.

Abstract

Proteins are essential components found in living organisms and play vital roles in various biological processes. Their significance is particularly evident in medical contexts, where the detection of proteins at extremely low concentrations, such as α-synuclein associated with diseases like Alzheimer's and Parkinson's, is crucial. Raman spectrum of proteins allows us to identify the chemical compounds based on their unique spectral fingerprint. However, the Raman effect is a relatively rare occurrence, making the detection of weak signals challenging.

To overcome the low Raman intensity, researchers employ surface-enhanced Raman spectroscopy (SERS), which enhances the Raman signal and enables the analysis of proteins even at low concentrations. Nonetheless, SERS substrates often exhibit fluctuations in intensity across their surface, primarily due to nonuniform distribution of field enhancement in the sample.

The objective of this research is to understand influence of the spatial intensity fluctuations on the Raman frequency, which is a measure of the protein conformation. In this project, we use a plasmonic nanostructure that includes an array of the nanoparticles on top of a gold mirror to probe multistate vibrational modes of proteins. Studying the vibrational modes of the protein on plasmonic surfaces is crucial to understand the possible conformations of proteins on such surfaces, which are widely used for sensing and biomedical diagnosis.

In order to maintain stable bonding of the protein Bovine Serum Albumin (BSA) and ensure a consistent protein conformation on the surface, a self-assembled monolayer (SAM) surface is used as a mediator between the protein and gold surfaces. This SAM surface consists of regions with different characteristics, such as hydrophilic and hydrophobic properties, as well as neutral or charged traits.

The research findings shows that a closed hotspot without any linking molecules provides the most effective intensity enhancement. Therefore, it is recommended to utilize an open hotspot when applying a self-assembled monolayer. Furthermore, the research demonstrates that α-helices remain intact only in coupled plasmonic nanocavities when neutral linking molecules are employed. In the case of both charged and neutral linking molecules, the surrounding environment exposes the side chains Tyr, Phe, and Trp. In case of particularly positive charged and neutral linking molecules, the α-helices are transformed into β-sheets.

Contents

List of abbrevations

BSA	Bovine Serum Albumin
MPA	3-Mercaptopropionic Acid
MUD	11-Mercapto-1-undecanol
Cys	Cysteamine hydrochloride
Phe	Phenylalanine
Tyr	Tyrosine
Trp	Tryptophan

1 Introduction

Raman spectroscopy is a spectroscopic technique to measure vibrational modes exhibited by molecules. Upon exposing a molecule to laser irradiation, a substantial proportion, exceeding 99 percent of the scattered light has the same frequency. This elastic scattering is called Rayleigh scattering. Conversely, a minute fraction of less than one percent, deviates from this frequency. That inelastic scattering is called Raman scattering. Raman spectroscopy can identify the chemical compounds based on the unique spectral fingerprint of each molecule. However, the Raman effect is a relatively low probability event making it challenging to detect weak signals.(1)

To enhance the detection sensitivity, the use of a metallic surface is necessary. This technique, known as surface-enhanced Raman spectroscopy (SERS), effectively amplifies the Raman signal, thereby facilitating the analysis of low concentrations of proteins.(2) Metallic substrates are extensively used in the realm of SERS owing to their ability to facilitate highly sensitive detection and imaging of molecules. SERS is applied in the diagnosis of cancers(3) and diabetes(4), but also for sensitive detection of viruses e.g. influenza(5) and COVID-19(6).

Nevertheless, SERS substrates exhibit a constraint of spatial fluctuations in SERS intensity. These fluctuations are frequently ascribed to nonuniform field enhancement(7) distribution of the sample. Additional explanations attribute these observations to the existence of picocavities and charge transfer phenomena occurring between the metal and the molecules. Using more complex biomolecules, these intensity fluctuations are even more unpredictable, especially for proteins.

Proteins are essential components of living organisms which play crucial roles in various biological processes. The structure of a protein can be categorized into primary, secondary, tertiary, and quaternary structures. A primary structure consists of a linear chain of amino acids. The secondary structure of a protein refers to the repeated arrangement of its backbone atoms. The most common types are α-helices, β-sheets and random coils(8), which are formed and stabilized by hydrogen bonds from the polypeptide backbone.(9) Fig. 1 shows a number of proteins that are characterized by the types of secondary structures. A part of the amino acid forms the polypeptide backbone of the protein. The rest of the amino acid is considered a side chain of the backbone and is called residues (R). The amino acids tyrosine, phenylalanine and tryptophan have large ring structures in their R groups, which make the side chain larger compared to those of other amino acids.(10)

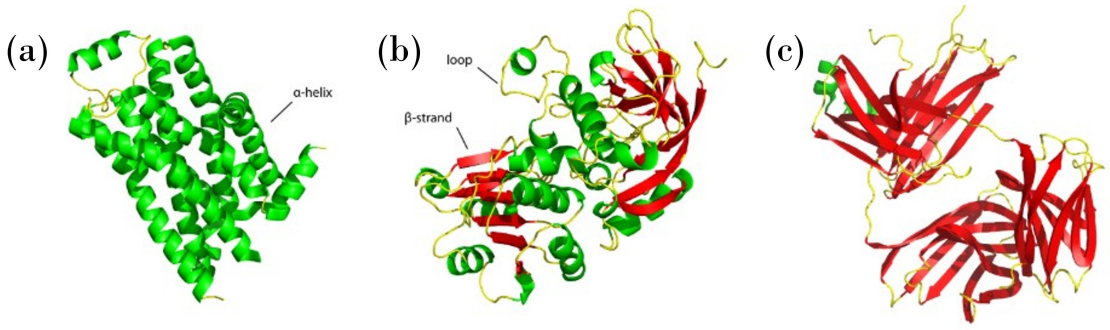

Figure 1: Examples of some proteins, containing different types of the secondary structure. (a) β_1 adrenergic receptor is made entirely of α-helices, (b) alcohol dehydrogenase has a mixture of both α-helices and β-sheets and (c) antibodies contain almost exclusively β-sheets. The α-helices are shown in green, β-sheets are shown in red and the loops are shown in yellow.(10)

There are some challenges in performing SERS measurements of biomolecules, especially for proteins. In many cases, it is necessary to create aggregates of nanostructures to generate high local fields which are suitable for SERS. When using aggregates of nanostructures, the obtained SERS spectra contain notable variations in both enhancement and spectral characteristics, which arise from the diverse interactions of the protein molecule with the nanoparticles, influenced by changes in protein concentration.(11) Due to the various possible orientations of adsorbed proteins, the SERS spectral reproducibility is a limiting issue for using plasmonic surfaces for sensing proteins and their conformations.(12) Moreover, direct contact between proteins and metal substrates often leads to protein denaturation.(13) Self-assembled monolayer could control the orientation of the proteins. However, it remains unclear how this approach would create an environment with coupled plasmonic nanocavities.

It is crucial to be able to make accurate measurements. For example, in a medical context it is very important to be able to detect proteins in extremely small concentrations. Specifically, α-synuclein, a protein associated with diseases such as Alzheimer's and Parkinson's, warrants detection at a very low concentration.

The objective of this research is comprehend the influence of the spatial intensity fluctuations on the Raman frequency, which is a measure of the protein conformation. This includes fabricating own samples with nanoparticle aggregates, a self-assembled monolayer and proteins. The optical part is also crucial, the measurements must be performed correctly. Finally, the analysis must ensure that only real Raman peaks are presented, without noise for example. Research will be done in the literature on how bonds within proteins are visible in the Raman spectrum.

1.1 Research Questions

The main research question of this project is: *How are molecular vibrations of proteins modified by a plasmonic surface?* Besides the main question, a number of sub-questions have been formulated to answer the main question.

- How does the sample configuration influences the SERS intensity and Raman wavelength fluctuations?
- How can the molecular vibrations be influenced by different linking molecules?
- What is the role of different protein conformations and side groups to the Raman spectrum?

2 Theory

Surface-enhanced Raman scattering (SERS) is a widely used spectroscopy technique. It offers highly sensitivity and it possesses the ability to amplify incident light which leads to a SERS enhancement exceeding 10^8(2). This extremely high enhancement makes that SERS is very interesting in biosensing due to its high sensitivity. It can generate a complete fingerprint of a molecule and that it is a label-free detection method.(7). For example SERS biosensors can be used in detection of diseases e.g. Alzheimer disease, Parkinson's disease, diverse forms of cancer and glucose detection in the context of diabetes.(14) In order to form the necessary basis for surface-enhanced Raman spectroscopy, we summarize the fundamental of Raman spectroscopy, localized surface plasmons and field enhancement of plasmonic nanostructures.

2.1 Raman spectroscopy

To better understand the concept of SERS, first the basics of Raman will be explained. Raman spectroscopy is a technique based on the interaction between light and matter. An incident photon with energy hv will raise the molecule from the vibrational state to one of the virtual states in between the ground electronic state and the first excited electronic state, as can be seen in Fig. 2.

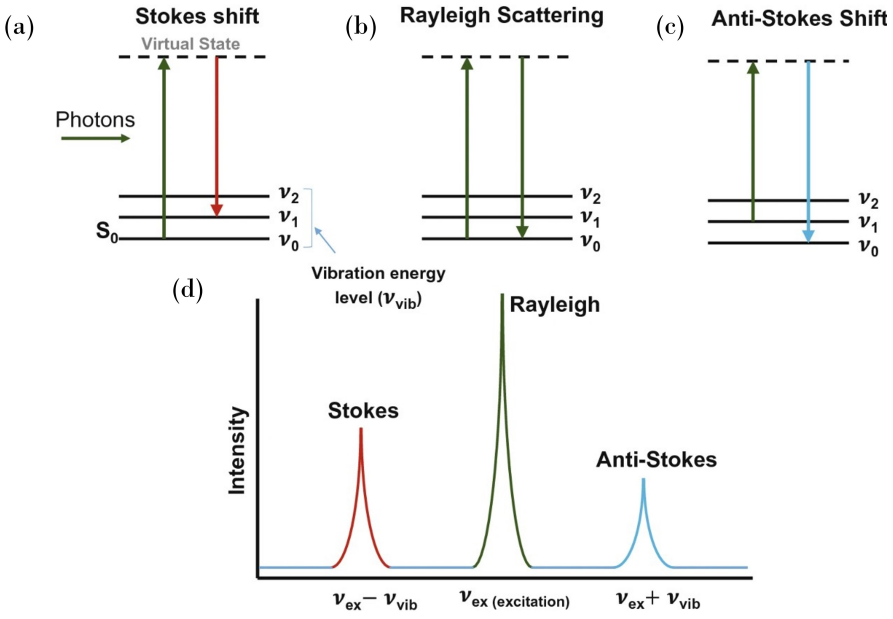

Figure 2: Energy-level diagram of (a) Stokes Raman scattering, (b) Rayleigh scattering, (c) anti-Stokes scattering. (d) Frequency comparison of Rayleigh, Stokes and Anti-Stokes scatterings. In (d) the intensities are not scaled. The photons are excited from a certain vibration energy level to the virtual state. Then they relax back to one of the vibration energy levels, which results in emitting of a photon with a different frequency for Raman scattering.(15)

In inelastic scattering, the incoming light has photons with a frequency ν_{ex}. Then the photon excites the molecule from S_0 to a virtual state before the photon is emitted. The emitted photon has an extra term in the frequency $\nu_{em} = \nu_{ex} \pm \nu_{vib}$. The extra term represent the phenomena called Stokes Raman scattering if the term is positive, and anti-Stokes Raman scattering if the term is negative.(2)

2.2 Localized Surface Plasmons

Localized Surface Plasmons (LSPs) refer to the collective oscillation of electrons confined at the surface of a metallic nanoparticle with a diameter smaller than the wavelength of light (Fig. 3). LSPs are induced by the interaction of incident light with the free electrons present in the surface of the metal, leading to the formation of localized electromagnetic fields. These plasmonic resonances can be observed as enhanced electromagnetic fields localized around the nanoparticle, resulting in unique optical properties. Several factors can influence the frequency of the oscillations, such as the shape and size of the charge distribution, the density of electrons and the effective electron mass.

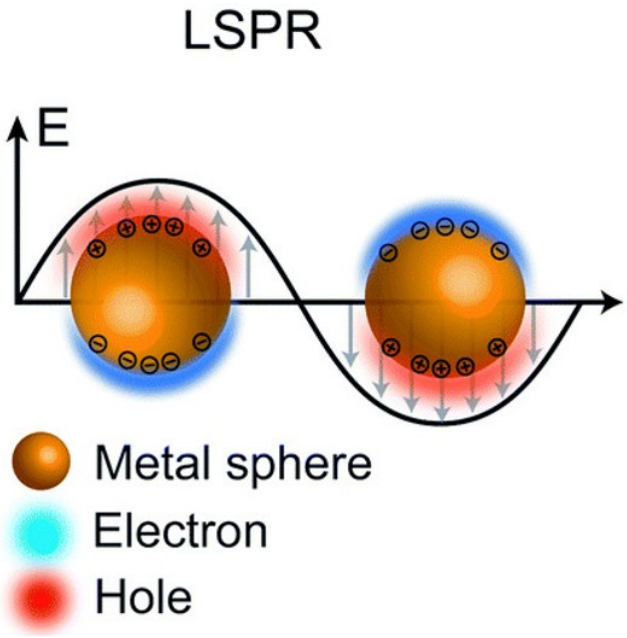

Figure 3: The oscillation of the free electrons at the surface of the metallic nanoparticle is shown. This oscillation is the origin of the field enhancement at the vicinity of the nanoparticle.(7)

2.3 Coupled plasmonic nanocavities

When an electric field interacts with plasmonic nanoparticles, the momentum of the electric field can be transferred to free electrons at the surface of the nanoparticle.(16) This transfer of momentum can induce the enhancement of electric fields in the vicinity of the particles. This field enhancement depends on the shape and material of the nanoparticles, and the surrounding medium.(17; 18) When placing two nanoparticles less than 2 *nm* to each other (Fig. 4a), the field enhancement can reach more than 100 times higher than that of a single nanoparticle.(19) Another structure is the nanoparticle on mirror (NPoM, see Fig. 4b). The nanoparticle is positioned on a metallic mirror, which leads to a coupling between the nanoparticle and its image charge in the mirror. This results to a similar enhancement as nanoparticle dimers.(20) In this research, we employ a structure consisting of an array of nanoparticles on top of the mirror, known as coupled plasmonic nanocavities (Fig. 4c). In this arrangement, the field enhancement is higher compared to NPoM due to the coupling between nanoparticles and their mutual interactions with image charges in the mirror. In this work we use coupled plasmonic nanocavities to study proteins.

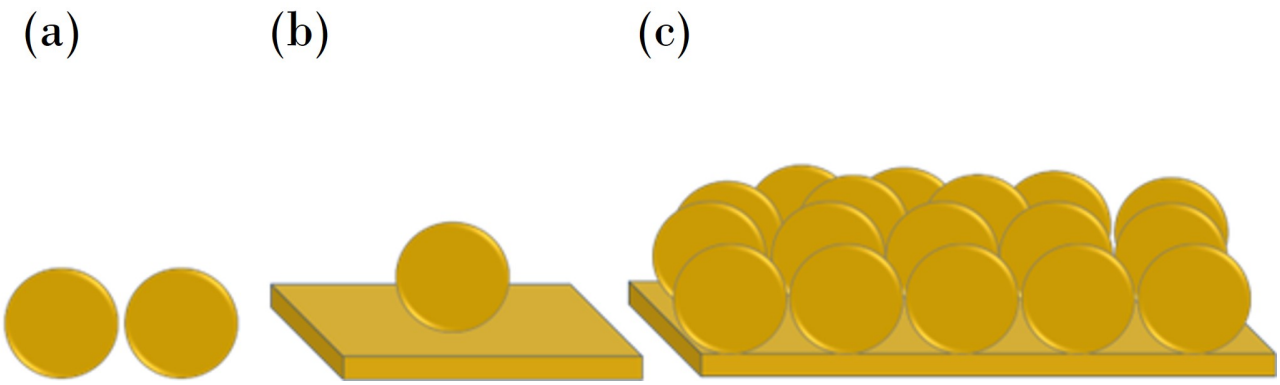

Figure 4: Different structures of nanoparticles, which are (a) two nanoparticles next two each other, (b) plasmonic nanocavity and (c) coupled plasmonic nanocavities.

In coupled plasmonic naonocavities, the field that is enhanced is confined between the nanoparticles and the gold film, and in between the nanoparticles. The SERS enhancement factor can be calculated by: $SSEF_{ex} = [E_{loc}(\omega_0)/E_0(\omega_0)]^4$.(7), in which E_{loc} is the local EM field and E_0 is the EM field of the incoming light. It should be noted the SERS enhancement factor is proportional to the electric field to the power 4. Any small changes in the field enhancement result into a significant change in the SERS enhancement factor. So if the samples is distributed non-uniformly on the gold nanoparticle aggregates, it experiences different field enhancement. Consequently, there is a variation in the SERS spectrum intensity.(7)

Based on these two field enhancements, the protein can be positioned in different ways. The protein can be added on the nanoparticles (open hotspot) or in between the gold film and the nanoparticles (closed hotspot). The open hotspot utilizes the field enhancement in between the nanoparticles. In addition, the closed hotspot also uses the field enhancement between the nanoparticles and gold film.

Raman peaks in the spectrum of a protein provide valuable information about the secondary conformation.(21) This is because the secondary structure of a protein is associated with vibrational modes of the peptide backbone and the side chains of amino acids. Those vibrational modes are sensitive to the local environment and bindings within the protein molecule. Raman spectroscopy measures the molecular vibrations which are triggered by the inelastic scattering of photons.

2.4 Bovine Serum Albumin (BSA)

BSA has widespread use as a model protein for investigating various biological processes, including protein folding, stability, and interactions. Additionally, BSA has structural similarities to human serum albumin make it relevant for understanding drug binding and transport mechanisms. BSA is about 8.3 nm in a compact state, to 26.7 nm in an extended state.(22). The protein and its domains are shown in Fig. 5. While domain 1 and 2 are very negatively charged, $-9e$ and $-7.8e$ respectively, domain 3 is slightly negatively charged, only $-1.3e$.(22)

BSA has different characteristic vibrational bands. The amide I and amide II bands are the main vibrational bands associated with the secondary structure. The amide I band arises from stretching vibrations of the carbon-oxygen double bond (C=O) and is typically found in the region of 1600–1690 cm^{-1}. The α-helix peak is

observed at 1653 cm^{-1}, as can be seen in Fig. 23 in the appendix. This peak can be attributed to the α-helix Amide I band component.(23; 24; 25) A helix made of more than six amino acids results in a characteristic band at 1655(26), while helices made of less than six amino acids would result in multiple peaks. There is a downshift of 10 cm^{-1} when some helices make coiled motifs.(25) Also an increase in strength of hydrogen-bonding results in a downshift in the frequency.(27) Next to the α-helix, there are some peaks related to the β-sheets, which results in a peak at 1670 cm^{-1} and a smaller peak around 1630 cm^{-1}.(25; 23) The amide II band, located in the range of 1480–1580 cm^{-1}, is primarily a result of in-plane bending of the nitrogen-hydrogen bonds (NH) and stretching vibrations of carbon-nitrogen bonds (CN). Compared to the amide I band, the amide II band is less sensitive to conformational changes in the protein.(8) According to different studies, BSA proteins in solution contain 67% α-helices.(24; 28; 29). It also contains around 30% β-sheets and some β-turns.(8)

In addition, BSA has several side groups: phenylalanine, tryptophan, tyrosine and histidine. In tryptophan there is an indole ring vibration which can give an intense peak around 1550-1555 cm^{-1}. BSA also has 24 residues of phenylalanine which gives a vibration 1586 cm^{-1} at and 1610 cm^{-1}. The aromatic ring of tyrosine results in a peak at 1613. cm^{-1}(25) The assignments of Raman bands are summarized in table 4.

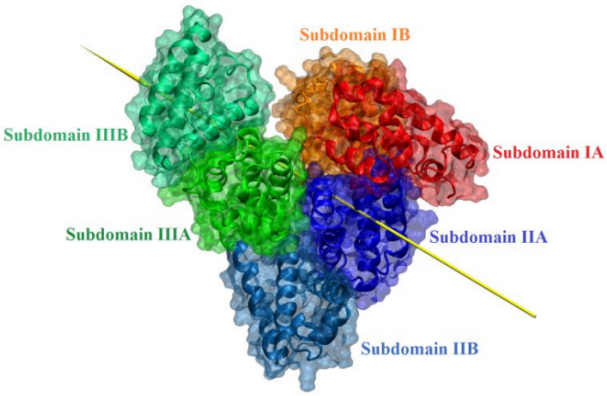

Figure 5: 3D structure of the BSA protein. Different colors shows the different subdomains of BSA.(30)

Table 1: A list of Raman bands and their structures.(25; 31)

Band	**Raman shift (cm^{-1})**	**Assignments**
Amide I	1670 (32)	β-turn, random structure
	1660 - 1670 (33; 34)	β-sheet
	1650 - 1655 (25)	α-helices
	1640 - 1650 (35)	random coil
	1630 (25; 34)	β-sheet
Amide II	1550	Very weak in Raman
Phenylalanine	1586 (36; 37; 38)	phenyl ring bond-stretching vibrations (out-of-phase)
	1606 (36; 37; 38; 39)	phenyl ring bond-stretching vibrations (in-phase)
Tyrosine	1613 - 1616 (38; 39)	sensitive to changes in hydrogen bond strength with water
	1604 (38)	sensitive to changes in pH
Tryptophan	1550 - 1555 (36; 38; 11; 39)	affected by the torsion angle

2.5 Protein adsorption

An important aspect in this research is the protein adsorption on the surface of a gold thin film and self-assembled monolayer surfaces with nanoparticles. This is because the adsorption depends on various adsorption properties, for example electrostatic interactions, hydrophobic and hydrophilic interactions.(40) If a protein is on the surface, various processes can still take place that can influence the adsorption. The protein can start to reorient itself and conformational changes can take place. In general, BSA is a stable protein and is soluble in water, making it a suitable protein for adsorption studies. It will be negatively charged at neutral pH. During the self-assembly of the monolayers, various linking molecules can be added, which influence the attachment of the protein. The terminal functional groups of the linking molecules are responsible for the differences in hydrophobicity. In addition, the linking molecules can be positively charged, negatively charged and neutral under the neutral pH conditions. These mechanisms are responsible for protein adsorption. Phan et al.(40) found that the adsorption of positively charged linking molecules is the best, followed by negatively charged linking molecules and worst for the neutral ones. The responsible mechanism in the charged molecules was the electrostatic interactions, while in the neutral molecules it is the hydrogen bonds. Hydrophobicity also played a role; a hydrophobic tail group works better. However, it is unclear how it behaves in SERS.

3 Experimental methods

In this section, we present a comprehensive overview of the systematic approach, sample fabrication process, setup details, and analysis methods employed in the study. The primary objective of this section is to obtain accurate measurements for further analysis and interpretation. To achieve this goal, it is essential to carefully fabricate the samples before conducting any measurements. In the subsequent section, we provide a detailed explanation of the various fabrication processes involved. Following that, we delve into the measurement procedures employed in our study, highlighting the techniques utilized to ensure precise and reliable data collection. Lastly, we discuss the analytical methods utilized to interpret and derive meaningful insights from the obtained results.

3.1 Methodological approach

To investigate the scientific problem and to link the results to a certain parameter, two different structures namely open and closed hotspot are used. We perform a systematic measurement to investigate the effect of open and closed hotspot, and various linking molecules. Part 1 is mainly focused on which arrangement would give the best enhancement, so the SERS intensities will be analyzed. Part 2 is mainly focused on which Raman shifts the peak is localized, so the Raman shifts will be analyzed.

Part 1: which arrangement gives the best enhancement?

- Open / closed hotspot with linking molecules
- Open / closed hotspot without linking molecules

Part 2: how is the Raman shift influenced by changes in molecular vibrations?

- Positive, negative and neutral linking molecules
- No linking molecules

3.1.1 Open hotspot and closed hotspot

There are two arrangements to use coupled plasmonic nanocavities. In *open hotspot* arrangement, the sample is placed on top of the nanoparticles aggregates (Fig. 6a,c). When the protein is placed in between the thin gold film and the nanoparticles, the arrangement is called *closed hotspot* (Fig. 6b,d). To investigate closed and open hotspots, we used structures with and without the linking molecule. Therefore, the structures that we investigates, are listed below.

- Open hotspot: Au thin film - Nanoparticles - BSA (Fig. 6a)
- Closed hotspot: Au thin film - BSA - Nanoparticles (Fig. 6b)
- Open hotspot: Au thin film - Nanoparticles - Cys - BSA (Fig. 6c)
- Closed hotspot: Au thin film - Cys - BSA - Nanoparticles (Fig. 6d)

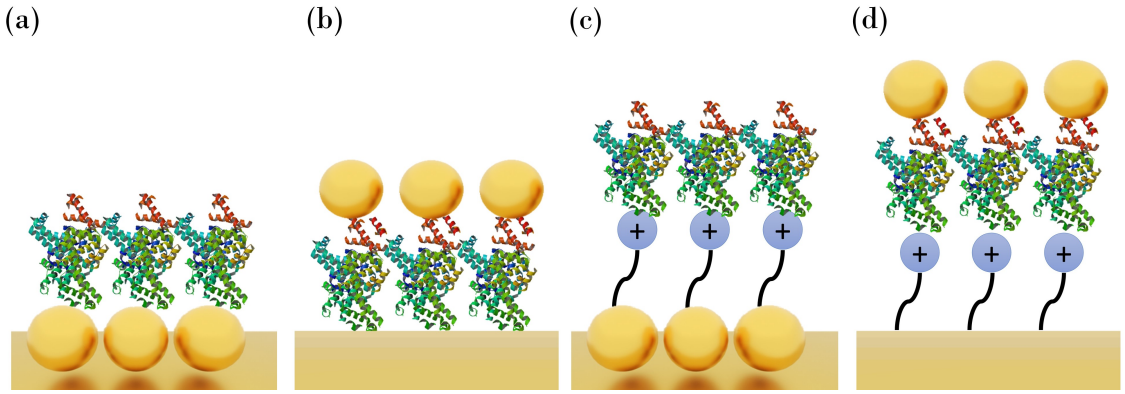

Figure 6: A schematic of the (a) open hotspot without any linking molecules, (b) closed hotspot without any linking molecules, (c) open hotspot with positive linking molecules and (d) closed hotspot with positive linking molecules. These representations are not to scale.

3.1.2 Different self-assembled monolayers in an open hotspot

In this research, we employed self-assembled monolayers (SAMs), assembled on the gold surfaces to provide soft landing for the proteins. It ensures consistent attachment of the protein to the nanoparticles. Different linking molecules are used to investigate the influence on the molecular vibrations and the protein adsorption. Positively and negatively charged linking molecules are used, and neutral linking molecules. Moreover, a sample without any linking molecule is investigated to be compared with the samples with the linking molecules. The investigated samples are:

- Negative MPA (Fig. 7a)
- Positive Cys (Fig. 7b)
- Neutral MUD (Fig. 7c)
- No linking molecules (Fig. 7d)

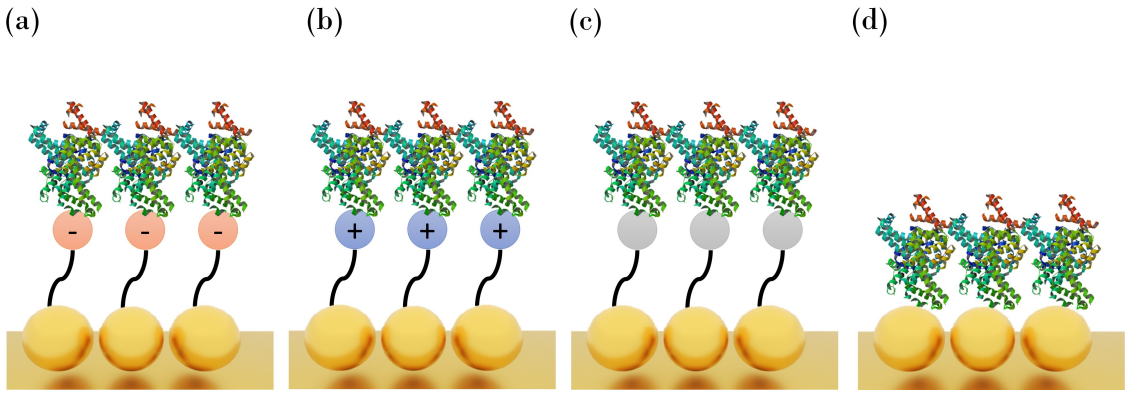

Figure 7: A schematic of the structures used to investigated the effect of linking molecules. (a) Open hotspot with negative linking molecules, (b) open hotspot with positive linking molecules, (c) open hotspot with neutral linking molecules and (d) open hotspot without any linking molecules. These representations are not to scale.

3.2 Sample fabrication

To fabricate coupled plasmonic nanocavities, a 100 *nm* thin gold film is provided using template stripping method. Also, the nanoparticle aggregates is fabricated and placed on top of the gold film. Depends on the structure of interest, the linking molecule is formed on top of the aggregation or on top of the gold film. The details of sample fabricating is discussed later.

3.2.1 Template stripping

The first step to fabricate coupled plasmonic nanocavities, is preparing the gold film, which will become the bottom layer of the sample. In other applications of gold thin films, coating techniques do namely not provide a flat surface in a large area. For preparing the thin film, we use template stripping method (Fig. 8) to provide a flat and smooth surface. Doing this, epoxy is applied to the rough gold layer and covered with a glass cover. After harden the epoxy with UV-radiation, the sample can be peeled off and the result is a smooth gold layer which can be used to fabricate the coupled plasmonic nanocavities. The standard deviation of the roughness is measured, which is 0.1 *nm* (see Fig. 24 in appendix A). This is possible due to the atomically flat surface of the silicon wafer.

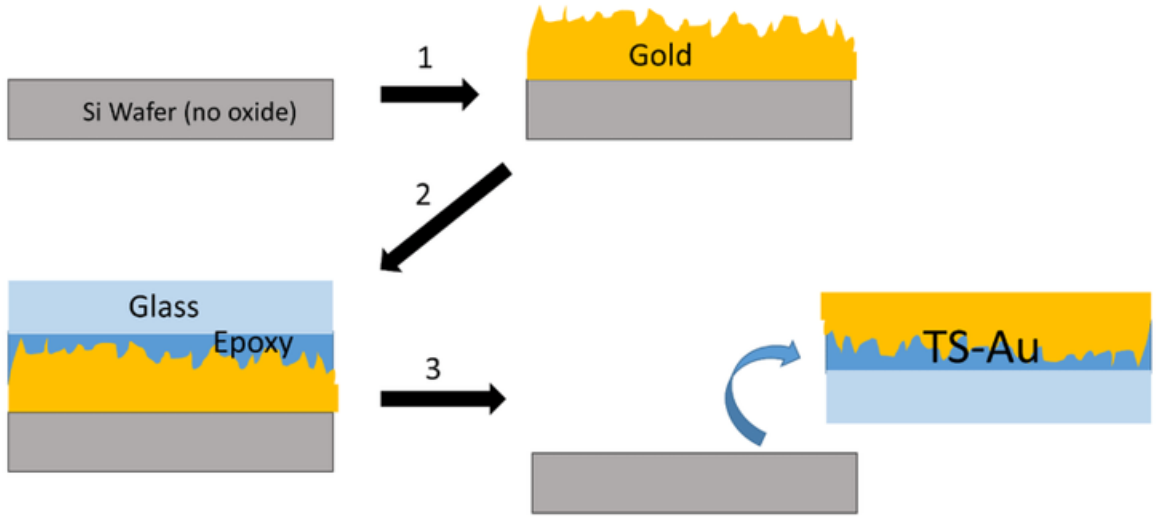

Figure 8: In step 2, a glass is glued to the gold thin layer with UV epoxy. In step 3, once the epoxy has cured, the thin gold layer can be scraped off the silicone wafer. The end product is a smooth gold thin film. (41)

3.2.2 Self-assembly of gold aggregation

For fabricating the samples, a strict protocol has to be followed.(42) To prevent impurities on the sample, work with gloves and clean the equipment such as tweezers and glasses before using them. For each sample, we need 1.0 *mL* hexane, a mix of 0.5 *mL* butylamine and 0.5 *mL* ethanol, and a mix of 1.0 *mL* gold nanoparticles and 1.0 *mL* ethanol. Hexane was used to get a monolayer of nanoparticles. With the aid of ethanol, the nanoparticles slowly float towards the interface forming a monolayer.(43) To ensure that the nanoparticle solution is uniform, the vial with the nanoparticles was shaken well before use. To remove the citrates, the nanoparticles was mixed with ethanol and centrifuging it till the nanoparticles are settled to the bottom. Now 1 *mL* of the liquid was taken out, which should be as transparent as possible so it does not contains the nanoparticles. The nanoparticles

was mixed again to get a uniform solution. Once the solutions are prepared, the components can be pipetted in the in-house fabricated chamber onto the gold thin film: first the nanoparticles, then the butylamine and finally the hexane. It is recommended to not mix it more than twice, otherwise the nanoparticles will clump together too much. After that, leave it for two hours to get the monolayer nanoparticles. The detailed protocol of this procedure can be found in appendix B.1.

3.2.3 Adding the linking molecules and protein

To complete the sample, the linking molecules and proteins have to be soaked in the sample. For the samples on which a SAM is desired, first the linking molecule has to be soaked on the sample. After 24 hours, rinse the sample with ethanol and then the protein has to be soaked on the sample for another 24 hours. The detailed protocol of this procedure can be found in appendix B.2.

3.2.4 Chemicals

Hexane (Sigma: 650552) and ethanol (Supelco: 1.00983) are used pure. Butylamine (Sigma: 471305) has to be diluted to 1 mM with demineralized water, which has to be done in two steps. In the process, it is used as a reductant.(44) Lastly, nanoparticles (BBI: EM.GC80) are used, with a diameter of 80 nm and an optical density of 1. The nanoparticles contain citrates on its surface, to prevent the nanoparticles clumping together. Adding ethanol to the nanoparticles causes the citrates to detach from the nanoparticles.

In this study, we employed BSA for investigating coupled plasmonic nanocavities. The BSA solution was prepared by dissolving BSA powder (Sigma: A7906) in demineralized water. It is crucial to handle the solution with care, excessive shaking can result in protein denaturation. The linking molecules which are used in this investigation, are MPA, Cys and MUD. The negative charged MPA (Sigma: M5801) was diluted to a concentration of 1 mM using ethanol (Supelco: 1.00983). The positive charged Cys solution of 1 mM was prepared by dissolving the powder (Sigma: 49705) in ethanol. Similarly, the MUD solution was prepared by dissolving the powder (Sigma: 447528) in ethanol. The linking molecules and their properties are summarized in table 2.

Table 2: The used linking molecules and their properties

Full name	**Chemical formula**	**Properties**	**Length (Å)**
3-Mercaptopropionic acid (MPA)	$HSCH_2CH_2CO_2H$	Negative, hydrophilic	7.29
11-Mercapto-1-undecanol (MUD)	$HS(CH_2)_{11}OH$	Neutral, hydrophilic	20.15
Cysteamine hydrochloride (Cys)	$HSCH_2CH_2NH_2 \cdot HCl$	Positive, hydrophilic	5.83

3.3 SERS measurements

The experimental setup to measure the Raman spectrum of the samples and perform 2D XY scans, is shown in Fig. 9. The setup consists of three parts: an excitation source, a microscopy and a spectroscopy part. The excitation source is a 632.8 nm He-Ne laser, which is used to excite the sample. The laser has an output of 12 mW, but due to the clean-up laser filters and beamsplitters, the power of the laser that finally reaches the sample is about 90 μW. The microscopy part contains an objective lense with an numerical aperture of 0.8 with 100x magnification. There is a Basler camera connected to the microscope to capture darkfield images of the sample, whose dimensions are around 46 by 33 μm. Darkfield images show the scattering of nanoparticles,

making it particularly useful for sample focusing and identifying areas of gold NP aggregates. Finally, there is a spectrometer to measure the Raman spectrum of the sample, which contains a notch filter to filter the light with the same wavelength as the excitation source. The spectrometer gives spectra with a range of around 160 *nm*. We want a spectrum of BSA that represents the entire fingerprint region, which is typically between 300 till 1900 cm^{-1}. That is why a central wavelength of 720 *nm* is selected. The SERS spectra of an area up to 400 μm^2 are measured, with a step size of 200 *nm*. A 3D representation of the setup is shown in Fig. 28.

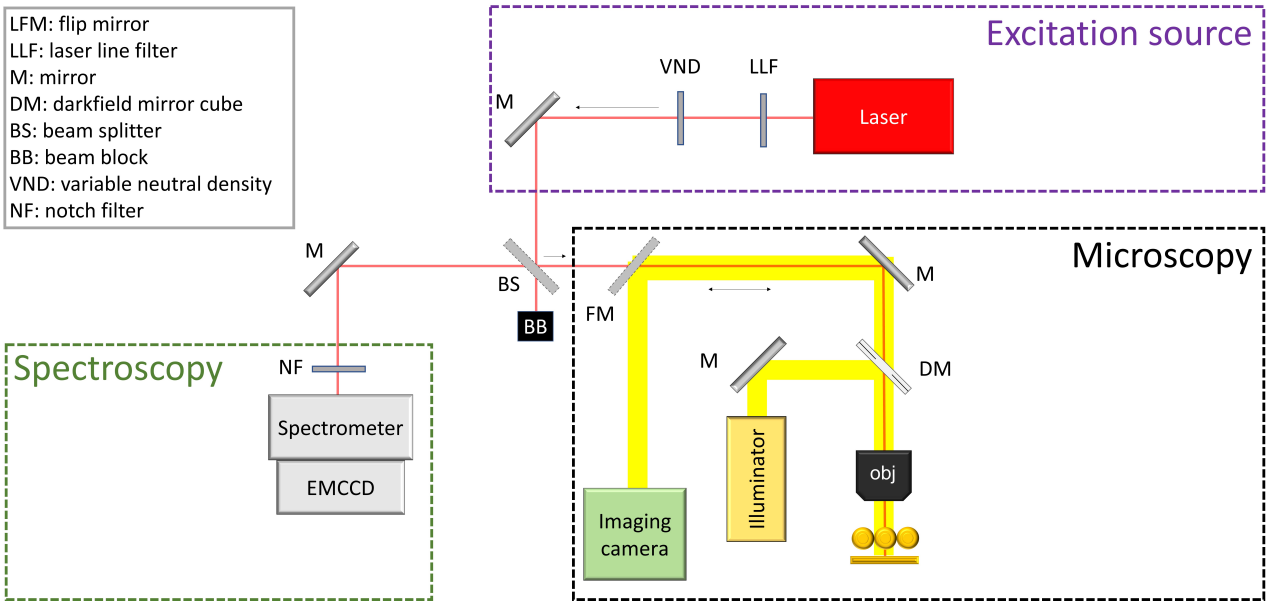

Figure 9: The setup, which consists of the excitation source, the microscope and the spectrometer.

3.4 Analysis procedure

Upon obtaining the raw Raman spectra from the spectrometer, the next step is to extract and analyze the data. This process starts with carefully examining the individual Raman spectra at a one-dimensional level, employing several processing techniques in order to recognize the real Raman peaks. These Raman peaks, which were derived through the utilization of an XY scanning technique, are subsequently shown in the form of two-dimensional (2D) maps. Lastly, other visualizations of the data are employed to obtain compact representations of the aforementioned 2D maps.

3.4.1 Raman spectra

The first step of analysing is to extract the raw data from the saved data file. A plot of the raw is made to observe if any signatures of BSA can be observed. Fig. 10 show two examples of the spectra measured by the spectrometer. To get the information about SERS intensities and Raman shifts of the sample, the raw data requires several steps for analysis. These steps include filtering the data, performing fitting procedures, identifying the Raman peak, and finally, plotting the results.

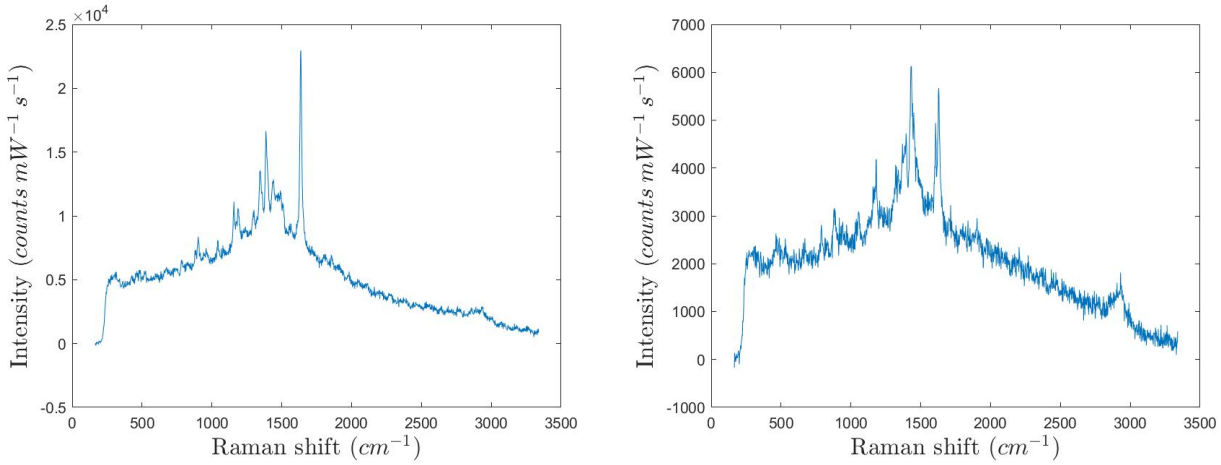

Figure 10: Two examples of the raw data measured by the spectrometer.

The first step is to remove the noise from the SERS signal and to create a Raman shift range. Noise has a high frequency compared to Raman peaks in the spectrum, so a low-pass Fourier filter is applied to filter out the noise. A low-pass filter only passes signals with a frequency below the passband frequency and attenuates all the signals above the frequency. The Raman signal will not be removed because it has a low frequency. Because the frequency range of interest is around the α-helix of the Amide I band, a range has to be applied around 1653 cm^{-1}. Different protein conformations changes could take place, so that has been taking into account with applying the range. The Raman peak for BSA, including eventual shift, will be in the range of about 1489 till 1830 cm^{-1}. In Fig. 11 the same data is shown as in Fig. 10, but now the low-pass filter and the range are applied.

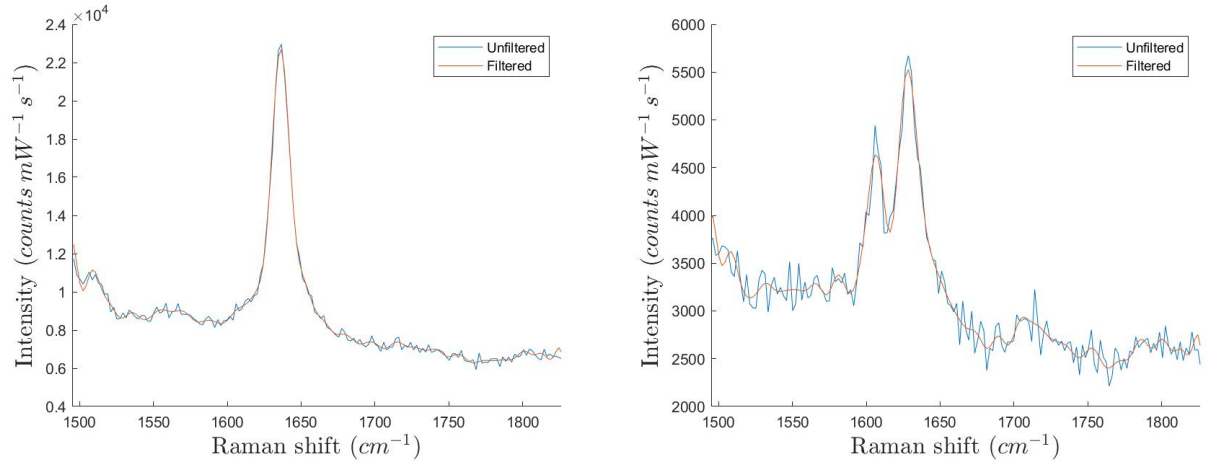

Figure 11: Blue: the unfiltered data to which the range has been applied. There is a lot of noise which a high frequency compared to that of Raman peaks. Orange: the data to which the lowpass filter as been applied. The noise is removed and the amplitude of the peak is not decreased.

Prior to extracting the Raman peak shift and SERS intensity, an essential preprocessing step involves removing the broad background of the spectrum, which is the background due to SERS enhancement. This is done to

ensure accurate measurement of the peak intensity. We achieve this by fitting a linear curve to the spectrum and subtracting it from the original SERS spectrum. As a result of this subtraction, the minimum value of the spectrum is approximately 0, indicating successful removal of the broad background, which can be observed in Fig. 12. Lastly, the peak position and intensity of all the peaks in the selected range is found. This is done using the *findpeaks* function, which is a built-in function in Matlab. This function searches for a defined number of peaks with a amplitude higher than a certain value.

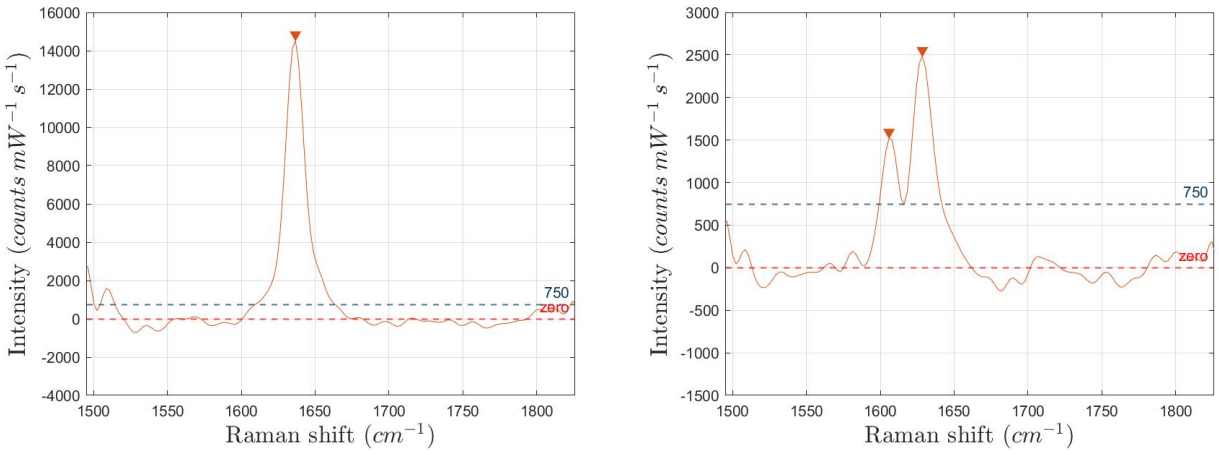

Figure 12: The data has been fitted. The peaks have been extracted and labelled, which will be used for further analysis.

3.5 2D representations

Once the peak is found, the SERS intensity and the Raman shift of the most intense peak at each XY location of the scanned area on the sample, will be presented in 2D maps. In the Raman shift maps, the relative Raman shift of the peak at each point on the surface will be presented. A blue color means that the most intense peak is blue-shifted compared to the BSA Raman shift value of 1653 cm^{-1}. A red color means that the peak is red-shifted. Also the SERS intensities of the Raman peaks will be presented in maps. A brighter color means a higher SERS intensity. When no signal is received by the spectroscope at a certain position, the corresponding spot will be appear white. At those positions, the Raman peak did not exceed the defined threshold. Also a darkfield image of the sample will be added, to observe some similarities between SERS intensities and the amount of nanoparticles aggregates.

3.6 Further analysis

To compactly represent the 2D maps, the results are further analyzed by making histograms of them. The SERS spectra of the BSA have up to three different peaks in the selected range. In Fig. 13 multiple Raman spectra after filtering and removing the broad background from the spectra, are presented which were taken at different XY positions on one sample. At a certain position on the surface, three peaks are detected (Fig. 13a), at another position on the same sample two peaks (Fig. 13b), at again another position only one peak is detected (Fig. 13c) and at another position there is not a single clear Raman peak is detected (Fig. 13d). Despite the spectra have been carefully observed in determining the threshold, the third peak may sometimes

be affected by the background. However, this may have occurred in a negligible number of spectra. A 2D map has been made of all first peaks (Fig. 14a) of the surface. In case there is a second and third peak in the spectrum, these peaks are also presented in a map (Fig. 14b,c). These maps are presented in a histograms (Fig. 14d-f). Then line graphs were made of these histograms, in order to get a representation of the three most intense peaks in one plot.

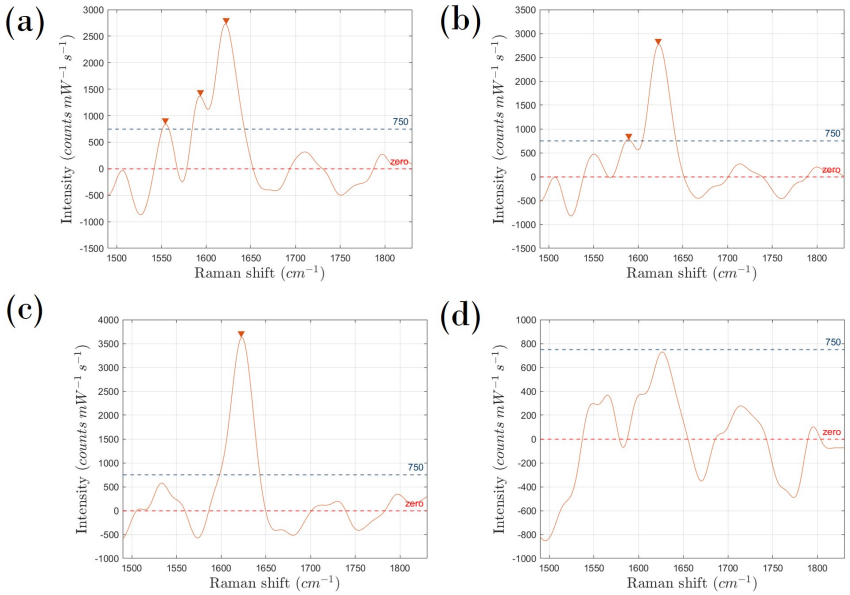

Figure 13: The filtered and fitted Raman spectra, which shows that in (a) there are three peaks detected, in (b) there are two peaks detected, in (c) there is only one peak detected and in (d) there are no peaks detected.

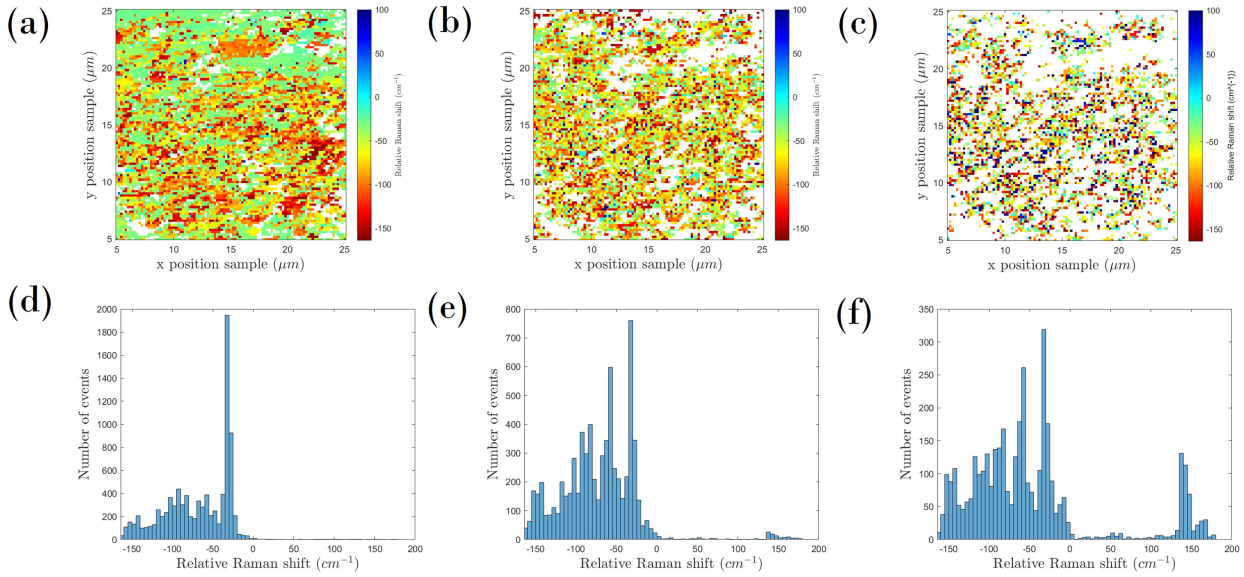

Figure 14: Each data point represents a peak which is in (a) the most intense peak, in (b) the second most intense peak and in (c) the third most intense peak. The histograms of the maps showed in (a-c), (d) the first intense peaks, (e) the second most intense peaks and (f) the third most intense peaks.

4 Results

In this section, the Raman shifts and SERS intensities of the peaks are presented in maps. To get a compact representation of the maps, they are visualized in histograms. First the results of the intensities using an open and closed hotspot are presented. After that, the results of the molecular vibrations using different linking molecules are presented

4.1 Raman imaging of proteins on plasmonic surfaces

Fig. 15 shows the 2D maps of a sample with BSA in an open hotspot, using negative linking molecules. First, no signal is received by the spectroscope at the spots that are white. This happens at spots where there seems to be no monolayer gold aggregates. Some similarities can also be seen between the Raman shift map (Fig. 15a) and the SERS intensity map (Fig. 15b). For example, the intense spot in the right side of the SERS intensity map seems to recur as a large negative in the Raman shift map.

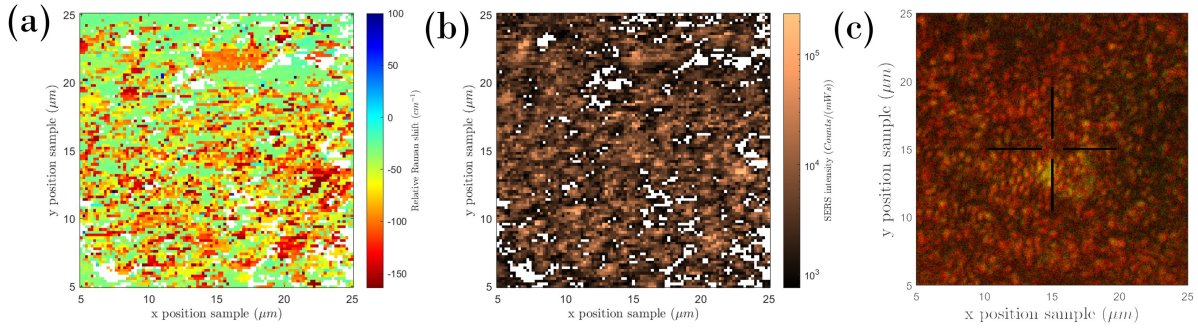

Figure 15: Each data point represents the (a) Raman shift or (b) SERS intensity of the most intense peak at a point (x,y). A blue color means that the most intense peak is blue-shifted compared to the BSA Raman shift value of 1653 cm^{-1}. A red color means that the peak is red-shifted. (c) The darkfield image of the scanned area.

In Fig. 16 the maps of a closed hotspot without linking molecules are presented. Figure 17 presents the maps of an open hotspot without linking molecules. A first impression is that more high intensities can be observed when using a closed hotspot, given the higher number of bright spots in Fig. 16b than in Fig. 17b. Also in these maps, a number of similarities can be seen between the Raman shift and the SERS intensity. The large bright spot in the upper left of Fig. 16b appears to reappear as a large negative shift in Fig. 16a. It again seems that the places where no monolayer can be seen in Fig. 16c do not result in an enhancement, which can be seen in Fig. 16b. For example, it appears that the nanoparticle aggregates on the right is not a uniform monolayer.

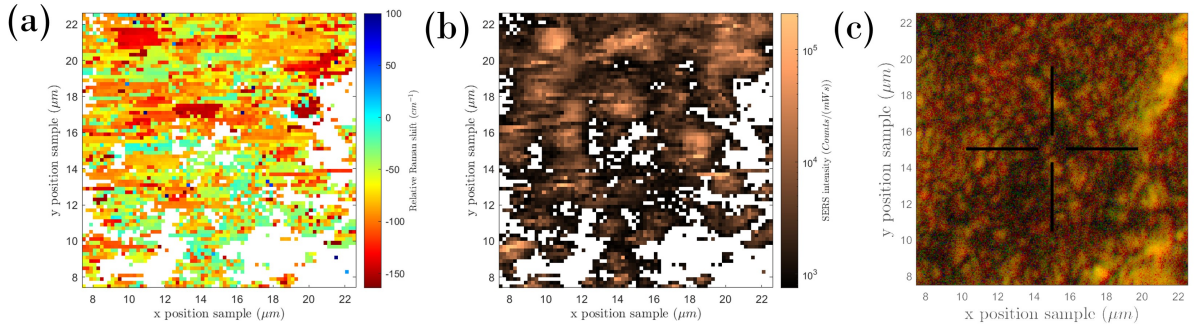

Figure 16: The (a) Raman shift map, (b) SERS intensity map and (c) darkfield image of the scanned area of a sample with BSA in a closed hotspot without using any linking molecules.

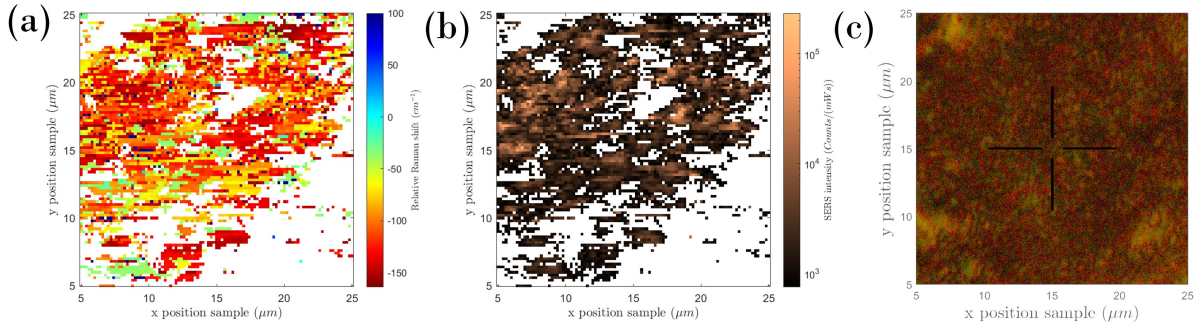

Figure 17: The (a) Raman shift map, (b) SERS intensity map and (c) darkfield image of the scanned area of a sample with BSA in an open hotspot without using any linking molecules.

4.2 SERS intensities using different sample configurations

The histograms in Fig. 19 shows the number of measured events of the intensity of the most intense peak of each spectrum, if it is at least 750 $counts\, mW^{-1}\, s^{-1}$. The upper quartile is indicated with a blue line. This means that 25% of the measured values are to the right of this line. If this value is relative high compared to the other upper quartiles, then high intensities have been measured more often. If this value is lower, high intensities have been measured less often. The values of these upper quartiles are summarized in table 3.

Table 3: Upper quartile per arrangement (the value of the blue lines in Fig. 19).

Hotspot	**SAM**	**Upper quartile** ($counts\, mW^{-1}\, s^{-1}$)
Open	Only BSA	3333
Closed	Only BSA	5310
Open	Cys + BSA	3250
Closed	Cys + BSA	2019

In case of open hotspot without using any linking molecules (Fig. 19a), the upper quartile is equal to 3329 $counts\,mW^{-1}\,s^{-1}$. In case of closed hotspot (Fig. 19b), it is at 5310 $counts\,mW^{-1}\,s^{-1}$. So it shows that a closed hotspot provide a higher SERS enhancement compared to open hotspot structure. However, when using Cys in a closed hotspot, no BSA signature is observed in the Raman spectra. This can be seen in Fig. 41a in appendix D. There is only a broad SERS background and no signature of BSA molecules in present. Without a signature of BSA, the variations in Raman shift when using different linking molecules cannot be investigated in the next part of this study. That is why we will continue this study with open hotspot structures.

4.3 Raman shifts using different sample configurations

In Fig. 18, the number of detected Raman shifts is presented in the case of an open hotspot and a closed hotspot structure. What can be seen in the case of both structures, is that there is a very wide band of frequencies in the negative range compared to the Raman shift of 1653 cm^{-1}. In addition, a Raman peak has often been detected at 1803 (+150) cm^{-1} in both cases.

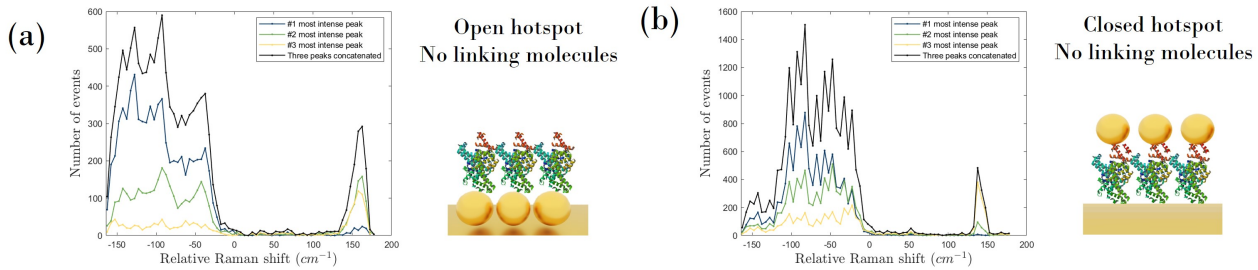

Figure 18: Raman shift of a sample with (a) an open hotspot structure and (b) a closed hotspot structure without using any linking molecules.

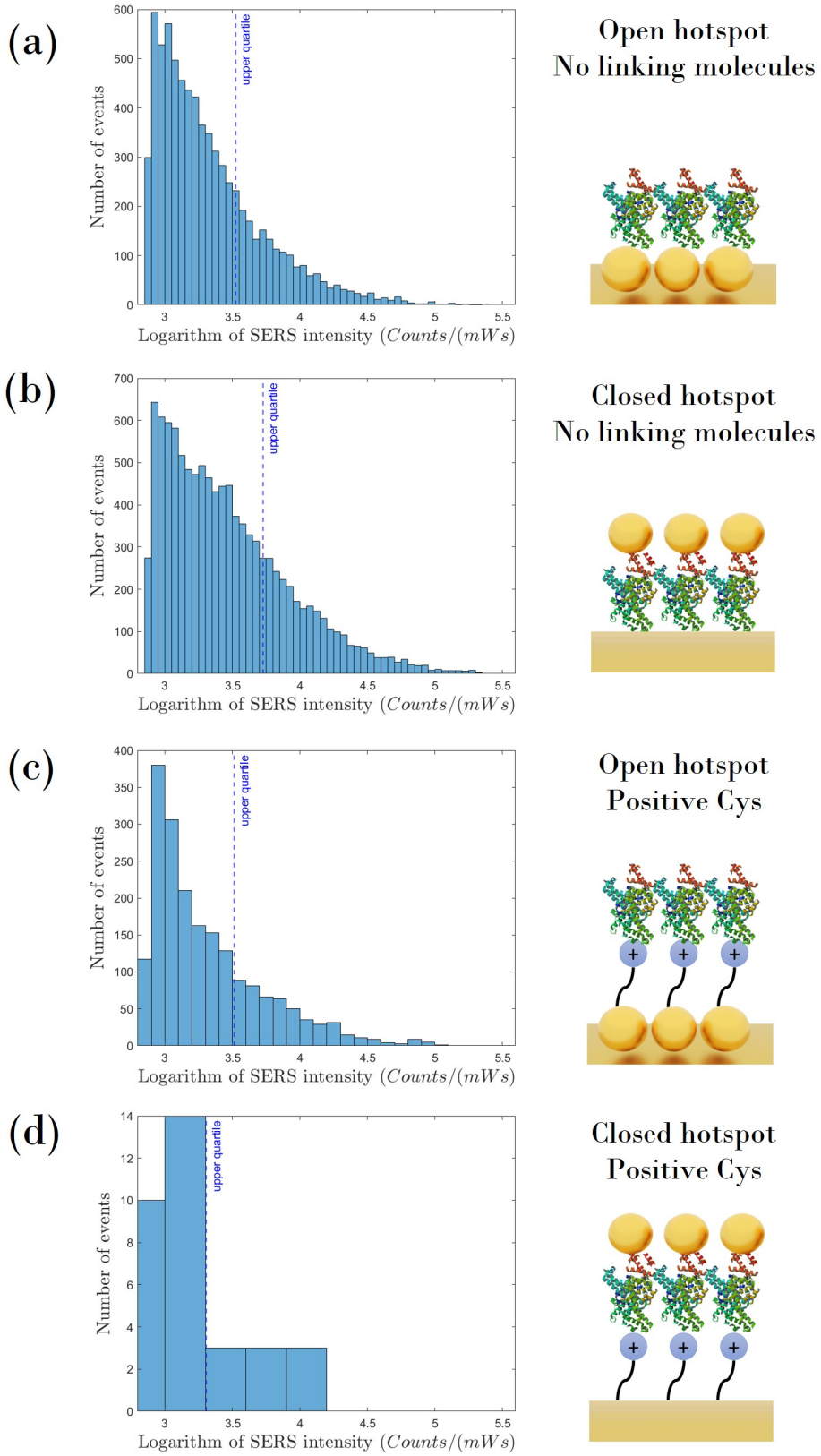

Figure 19: The histograms shows the number of events of measured intensities. The upper quartile is indicated with a blue line. This means that 25% of the measured values are to the right of this line. The values of the upper quartile are summarized in table 3. The cartoons next to it represent the sample that was used, which are not scaled.

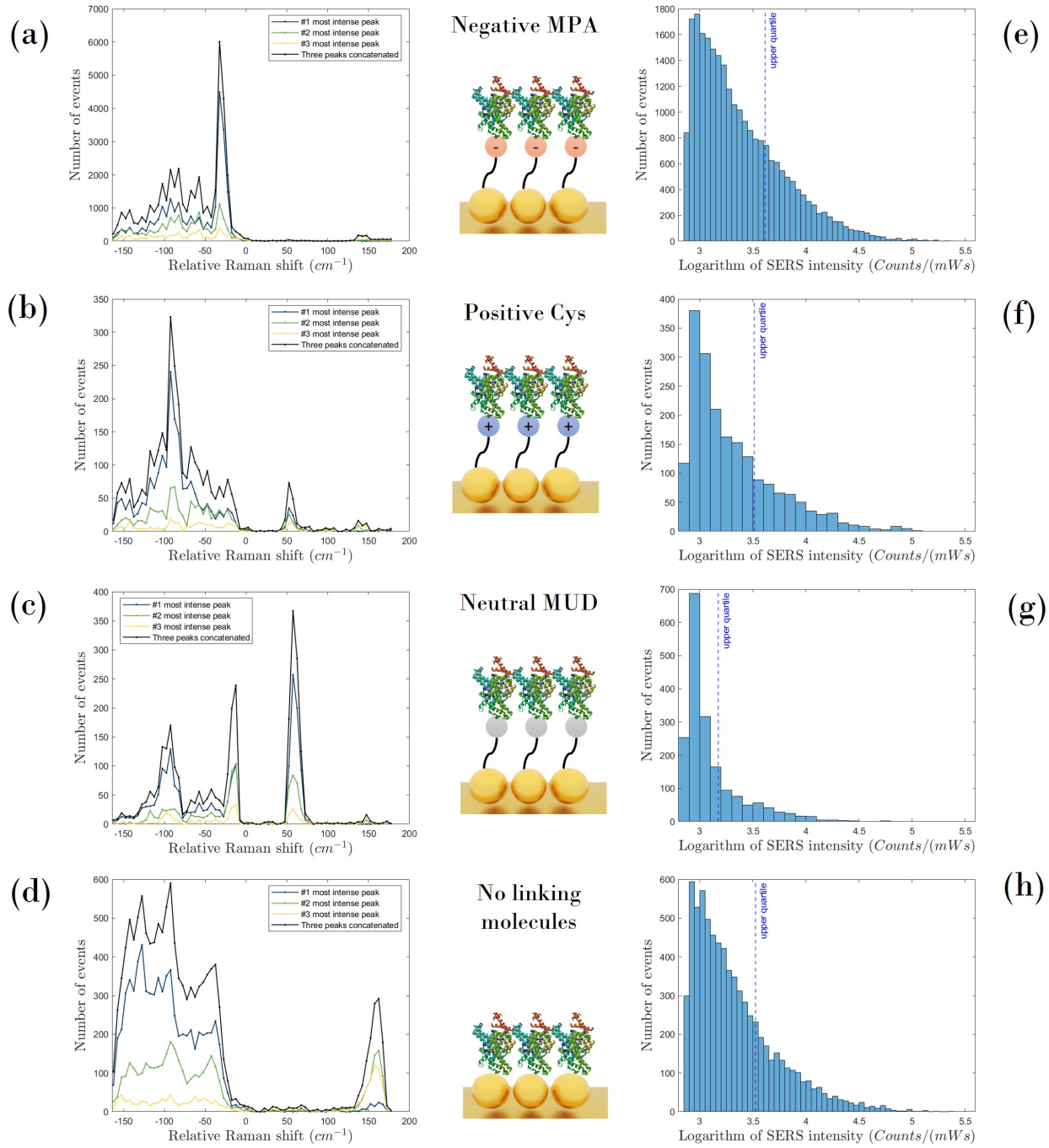

Figure 20: The line plots shows the number of events of measured relative Raman shifts. It is normalized to a Raman shift of 1653 cm^{-1}, which is equivalent to the α-helix in an Amide I band. The histograms shows the number of events of measured intensities. The upper quartile is indicated with a blue line. This means that 25% of the measured values are to the right of this line. The cartoons in between represent the sample that was used, which are not scaled.

4.4 Raman peaks using different linking molecules

The line plots in Fig. 20 show the number of events of a measured Raman shift, in the case of using the negative MPA (Fig. 20a), the positive Cys (Fig. 20b), the neutral MUD (Fig. 20c) and without any linking molecules (Fig. 20d). These line graphs are based on histograms of the Raman shifts of the peaks. Three peaks have been distinguished, from the most intense peaks (blue) to the 3rd most intense peak if any (yellow). These are added together which comes out to the black line. The peaks of those line plots are summarized in table 4. First the absolute Raman shifts are mentioned, then in brackets the relative shift compared to the reference.

Table 4: A list of detected Raman bands

SAM	**Raman shift** (cm^{-1})
MPA	1570.5 (-82.5)
	1620.5 (-32.5)
Cys	1560.5 (-92.5)
	1705.5 (+52.5)
MUD	1560.5 (-92.5)
	1640.5 (-12.5)
	1710.5 (+57.5)
Wtihout any linking molecules	1525.5 (-127.5)
	1560.5 (-92.5)
	1615.5 (-37.5)
	1815.5 (+162.5)

Using the negative MPA (Fig. 20a), there are many peaks of the Raman spectra detected at a Raman shift of 1620 (-33) cm^{-1}. Next to this peak, there is a shoulder of more peaks that are positioned on a more negative relative Raman shift. There are some small peaks protruding above the shoulder, namely at 1560 (-93) and 1570 (-83) cm^{-1}. However, the peaks at specifically these Raman shifts are detected less often than the Raman shift at 1620 cm^{-1}. Lastly, a very small number of peaks have been detected at 1803 (+150) cm^{-1}. It can also be noticed that there are almost only negative shifts. The reference peak at 1653 cm^{-1} is no longer detected.

Using the positive Cys (Fig. 20b), the most Raman spectra peaks are detected at a Raman shift of 1560 (-93) cm^{-1}. Again, there is a shoulder of more peaks around these main peak. These are positioned more negative as well as more positive compared to the main peak. Unlike the negative MPA, now there are some detected in the Raman spectra at a positive Raman shift, namely at 1705 (+52) cm^{-1}. Again, a very small number of peaks have been detected around a Raman shift of 1803 (+150) cm^{-1}. This one is not often detected, but it is a notable spike in the positive range.

Using the neutral linking molecule MUD (Fig. 20c), almost all of the Raman peaks are localized at one of three specific frequencies. These Raman peaks are located at a frequency, in order from less often measured to more often measured, 1560 (-93), 1640 (-13) and 1710 (+57) cm^{-1}. The neutral linking molecules is the only one of the linking molecules that results in Raman frequency close to the reference. The peaks of the Raman spectra are detected at specific frequencies. That can be seen from the peaks which are quite narrow. Moreover, almost no peaks have been measured in the frequencies in between. The only shoulder can be seen between the 1560 and 1640 cm^{-1}. Overall, it can be noticed that this neutral linking molecule contained the peaks that were also seen with the linking molecules discussed above, including the small number of peaks on a Raman shift of 1803 (+150) cm^{-1} that have been detected again.

Without using any linking molecules (Fig. 20d), there are a lot of Raman peaks measured in a broad range of Raman shifts in the negative range compared to the reference. These broad range of Raman shifts starts at a Raman shift 1630 (-23) to 1490 (-163) cm^{-1}. There are some outliers in this broad band, which are positioned at a Raman shift of 1615 (-38), 1560 (-93) and 1525 (-128) cm^{-1}. These outliers have been seen more often when linking molecules were used. Raman peaks were also detected at a high positive Raman shift, namely at 1815 (+162) cm^{-1}, but in this situation much more often compared to the previous situations.

4.5 SERS intensities using different linking molecules

Next to the line plots with the number of measured Raman shifts events in Fig. 20, the number of measured SERS intensity events of the most intense peak of each spectrum are visualized in histograms, if the Raman peak has a SERS intensity of at least 750 $counts\,mW^{-1}\,s^{-1}$. Again, the upper quartile is indicated with a blue line. Those values are summarized in table 5.

Table 5: Upper quartile per arrangement (the value of the blue lines in Fig. 20).

SAM	**Upper quartile** ($counts\,mW^{-1}\,s^{-1}$)
MPA	4119
Cys	3250
MUD	1485
Without any linking molecules	3333

What can be observed, is that using the neutral MUD (Fig. 20c) gives the lowest intensities, with an upper quartile of only 1485 $counts\,mW^{-1}\,s^{-1}$. Using the negative MPA (Fig. 20a) gives the highest upper quartile, with an upper quartile of 4119 $counts\,mW^{-1}\,s^{-1}$. In the case of the positive Cys (Fig. 20b) and when there are no linking molecules used (Fig. 20d), the upper quartile is approximately equal to each other, respectively 3250 $counts\,mW^{-1}\,s^{-1}$ and 3333 $counts\,mW^{-1}\,s^{-1}$.

5 Discussion

Now we got an overview with histograms to compactly present the SERS intensities, and line plots to compactly present the number of Raman peaks with a given Raman shift. First, the results of the intensities using an open as well as a closed hotspot will be discussed. After that, the results of the molecular vibrations using the different linking molecules.

5.1 Intensities of open and closed hotspots

In the results, we saw that a closed hotspot gives a better enhancement than using an open hotspot when there are no linking molecules used. This is consistent with the findings of Perez et al.(7), they also claimed that distance is an important factor. In the case of a closed hotspot, more BSA molecules will be positioned closer to the enhancement surface.

This comparison is also made using positive Cys molecules. What can be observed is that with an open hotspot (Fig. 19c) there is a similar result as when no linking molecule was used. Although there is now an extra length of almost 0.6 *nm* (see table 2) due to the linking molecules, the enhancement is still present. This is because the length of the positive linking molecule, which is around 0.6 *nm* is still within the optimal enhancement distance of 1 *nm*, according to the findings of Radzium et al.(45). It is known that the electric field decreases rapidly when the distance of the protein to the hotspot increases. As a result, only the molecules in close proximity to the substrate surface are detected.(12)

In the case of positively charged linking molecules in a closed hotspot, we found that there is only SERS background and no signature of BSA molecules in the Raman spectra. This is because it is unknown what happens to the protein in a closed hotspot structure. In the closed hotspot structure, there is a possibility to denature the protein in contact with the gold nanoparticles arrays. That was a reason to continue the research with an open hotspot when using different linking molecules, despite a closed hotspot potentially has higher SERS enhancement.

5.2 Intensities using different linking molecules

We found that the negative linking molecules MPA gave the highest intensities, followed by the positive Cys and MUD, giving slightly lower intensities compared using MPA. The neutral MUD gave the lowest intensities. A clear explanation for these is observations is that the neutral linking molecules are long; above 2 *nm*. This results in the fact that the BSA proteins are not in the field for an optimal enhancement anymore, so a longer distance to the hotspot results in a lower SERS intensity. In Fig. 27 in appendix A this phenomena is shown, where the field enhancement decreases as the distance becomes longer.

The other linking molecules have a comparable length; Cys is up to 0.6 *nm* long and MPA is up 0.8 *nm*. Although there is no extra distance when no linking molecules are used, the SERS intensities are still comparable because in all these cases the distance from the protein to the hotspot is within 1 *nm*. Then the field enhancement are similar for these structures, resulting in comparable SERS intensities.

5.3 Molecular vibrations using different linking molecules

In the results, we found interesting results about the Raman shifts. These are explained in this section by relating them to bonds and structures within a BSA protein.

5.3.1 Raman peaks and protein conformations

In the results, we saw that Raman peaks are located at different Raman shifts when different linking molecules are used in a coupled plasmonic nanostructure. The Raman peaks were compared to the reference of α-helix which is 1653 cm^{-1}. In most of the cases, mainly downshifts take place.

When the negative linking molecules MPA are used, we saw a lot of Raman peaks which are located at a Raman shift of 1620 cm^{-1}. This peak is related to the side group Tyr(38; 39), which is sensitive to changes in hydrogen bond strength in water.(25) This peak accompanies the low frequency β-sheet, which may fall in the peak. There are also peaks found at 1560 (-93) and 1570 (-83) cm^{-1}. The 1560 cm^{-1} peak can be related to the side group Trp(38; 11; 39), which is affected by the torsion angle. This is accompanied by the weak amide II bond. The 1570 cm^{-1} peak comes from the Phe side group(36; 38), which is an out-of-phase phenyl ring bond-stretching. These side groups (Phe, Tyr and Trp), which are also called aromatic amino acids (AAA) are more commonly associated with the emergence of β-sheets, according to the theory where the side groups are said to have more space and are able to occupy more space when surrounded with β-sheets, rather than α-helices.(46)

When the positive linking molecules Cys are used, we saw a high peak at 1560 (-93) cm^{-1}. That one was also visible when using the negative linking molecules, and is related to the side group Trp with the weak amide II bond. The shoulder around this peak also contains peaks from the other side groups. Jing et al.(47) found that the addition of positive metal ions lead to the exposure of aromatic amino residues. They also observed that Trp residues of BSA solution can exist in a hydrophilic environment and there is a conformational transformation of BSA from α-helix to β-sheets, due to a change of the hydrogen bond structures which induces the unfolding of α-helix structures. Our results indicates that there is indeed no α-helix, but instead indication of some β-sheets at low frequencies. There is another peak which belongs to the Amide I band in the positive range compared to the reference, which is from β-turn.

Table 6: A list of Raman bands and their structures.(25)

SAM	**Raman shift (cm^{-1})**	**Assignments**
MPA + BSA	1570.5 (-82.5)	Phe
	1620.5 (-32.5)	Tyr
Cys + BSA	1560.5 (-92.5)	Trp, Amide II
	1705.5 (+52.5)	β-sheet, β-turn
MUD + BSA	1560.5 (-92.5)	Trp, Amide II
	1640.5 (-12.5)	α-helix, with some coil motifs
	1710.5 (+57.5)	β-sheet, β-turn
Only BSA	1525.5 (-127.5)	unknown
	1560.5 (-92.5)	Trp, Amide II
	1615.5 (-37.5)	Tyr
	1815.5 (+162.5)	unknown

When the neutral linking molecules MUD are used, we saw very distinct peaks at 1560 (-93), 1640 (-13) and 1710 (+57) cm^{-1}. The peak at 1640 cm^{-1} is related to the native α-helix in combination with some random coil motifs.(25; 35) So only if neutral linking molecules are used, the native α-helix can only be observed in a coupled plasmonic nanostructure. Besides the α-helix, also the side groups and β-sheets gives a Raman signal at a high Raman shift.

When no linking molecules are used, there is a broad band of Raman shifts. It indicates that the protein cannot land softly and a modification is taking place by the gold nanoparticles. There are some outliers above the shoulder. Two of those outliers seem to be due to the side groups, namely the one at 1560 (-93) cm^{-1} and the one at 1615 (-38) cm^{-1}. In addition, there is another low Raman shift, at 1525 cm^{-1}, which cannot be directly related to side groups or Amide II. There is also a peak at 1815 cm^{-1}, which cannot be directly related either. This peak recurred in using any linking molecules, but to a lesser extent.

5.3.2 Denaturation

Several studies have investigated the denaturation of proteins. This study(48) measured a blue-shift of the α-helix from 1658 to 1667 cm^{-1}, when the temperature is increased from 25 to 85 °C. This suggests that the α-helix structure is transformed to a random coil or β-sheet.(49; 29; 25)

What also happens within a protein when it starts to denature is that hydrophobic groups normally buried on the inside of the protein are now exposed. This allows the aromatic amino acids to give off more detectable vibrations.(50; 51) Denaturation is also accompanied by a decrease in α-helices. This is also the case in the data presented, where we saw almost no α-helices, but a lot of signal from the side groups.

5.3.3 Reproducibility

What can be observed, is that using MPA gives a relatively high peak compared to the other samples. MPA provides a compact monolayer(40) that allows the protein to settle a stable conformation, which was also observed by Sivanesan et al.(52). Cai et al.(53) also found that a layer of negative molecules is useful to prevent the direct interaction of the proteins with a metal surface, with a remark that they used negative iodide ions instead of MPA. This protects the native structures of the protein to a certain extent. They found that it was very helpful for the compatibility, but the protein can still be uncontrollable. Xu et al.(54) came to the same conclusion; when proteins are in direct contact with the nanoparticles, using negative molecules seems to make the method more effective and reliable. This can greatly improve reproducibility and sensitivity.

Using Cys the most intenste peak is about 50 cm^{-1} more negative than the main peak when using MPA. In addition, there are more surrounding peaks. Guo et al. (8) observed an increase of β-sheets and a small increase of β-turns when positive calcium ions are added. These β-sheets and β-turns are responsible for the small peak at +50 cm^{-1}, and maybe also some lower frequency β-sheets in the negative region. The main peak at 1653 cm^{-1} disappeared, and several peaks around it replaced the main peak due to other conformations.

When neutral linking molecules are used, specific sites of the protein can be seen binding to the surface. This results in three clear pointed peaks. Since no charge is present, this phenomenon may be due to the polarizability. In the other cases, the charge will be dominant over the polarizability. When no linking molecules

are present, it can be seen that the molecule has no grip. It binds with the nanoparticles from all sides. It has no preference. It will not provide improved reliability and reproducibility.

5.4 Points of attention

During this study it has become apparent that one has to be very careful with optical and chemical procedures. To make self-assembled monolayers, the appropriate protocol must be strictly followed. The choice of gold in the samples improves chemical stability and prevents oxidation.(7) The samples were stored in a nitrogen environment to prevent chemical changes of the sample. Steps have also been followed when taking measurements to ensure that the setup is aligned. For example, a power measurement was taken before the measurement started. In addition, the position of the laser on the spectroscope has been checked whether it is centered. The position of the laser on the camera has also been checked to see if it is in the center and symmetrical.

Using SERS, small molecules can be observed as well as proteins can be detected. For small organic molecules, it would give a signature with peaks at a specific Raman shift, which can be observed in figure 25 when using methylene blue. The differences in wavelength are really small, within 0.3 nm due to the limited resolution of the spectroscope used. This means that the spectroscope has a good resolution. However, that 0.3 nm can cause a small offset in Raman shift of only 4.7 cm^{-1}.

There is a small difference ($< 10\ cm^{-1}$) in the absolute amide I peak in solution measurement and SERS measurement. This offset can be due different calibrations of the used spectroscopes. To get an idea of it; a Raman shift of 10 cm^{-1} is equal to only 0.41 nm.

5.5 Recommendations

Some improvements are possible to perform better analysis. At the moment it is more difficult to compare the intensities with each other. That's because the samples differ slightly in the density of the nanoparticles. It is also possible that the BSA coverage is not equal over the entire surface of the sample. For further research it is recommended that a uniformity of the substrate can be guaranteed, for example by using higher concentrations of linking molecules or a longer soaking time.

The result shows that positive linking molecules in a closed hotspot do not give a BSA signature. Therefore, it was decided to continue the research with an open hotspot. It is unclear which process is responsible for this, while a closed hotspot potentially gives higher intensities. Therefore, further research can be carried out into why this happens and how it can be prevented. An attempt can also be made to create both an open and a closed hotspot by adding the proteins before applying the nanoparticles and adding the proteins after applying the nanoparticles.

Moreover, the results can be confirmed by several methods. There are a number of bands at lower wave numbers that are characteristic of BSA. Amide III, for example, has a frequency of 1300 cm^{-1}. The side groups can also give multiple vibrations, including vibrations with a lower wave number of around 850 cm^{-1} in the case of Tyr. In addition, another protein can be investigated to compare the Raman peaks with BSA. Lysozyme proteins have a different conformation than BSA. These have fewer α-helices, fewer β-sheets, and more random

structures. They also have different residue groups. Lysozyme, for example, has much more Trp than BSA, so the peak at 1550 cm^{-1} will be larger in the case of lysozyme. BSA, on the other hand, has more Tyr compared to lysozyme, so that the frequency of 850 cm^{-1} mentioned in the previous section gives a more intense peak. Moreover, BSA contains 24 residues of Phe while lysozyme has only 3. This will give higher peaks at BSA on a number of frequencies, including at 1610 cm^{-1}.

In this study we used SERS. The results from this can be confirmed with other spectroscopic techniques. The conformations of proteins can be confirmed with Fourier transform infrared spectroscopy, which also detects vibrations like the SERS technique but is based on changes in dipoles instead of polarizability. In addition, the vibrations can be measured with an Atomic Force Microscope, provided the resolution is up to 1 nm. Contact angle measurements can also be performed to investigate the attachment of linking molecules. This directly says something about the hydrophobicity. If the angle is greater than 90 degrees, the linking molecule will have a hydrophobic terminal. If the angle is less than 90 degrees, it will have a hydrophilic terminal.(40) To compensate for the possible different calibrations of the used spectroscopes, it would be better that our laser intensity is higher so it also measure the reference Raman peak for BSA in solution.

6 Conclusion

In this research we first investigated to different plasmonic structures to detect the SERS signature of the protein. Results show that a closed hotspot without any linking molecules gives the highest SERS enhancement compared to open hotspot structure. Also, there is a possibility to denaturalize the protein due to its contact with gold surfaces of the nanoparticles array. To avoid any denaturalization of protein and ensure a consistent attachment of the protein, we use a SAM monolayer as a linking molecule.

In the second part of this research, we use different charged linking molecule including negatively charged, positively charged and neutral. A BSA protein was used as a sample and the spatial intensity and spatial frequency of the BSA is characterized by fabricated coupled plasmonic nanocavities. We use the peak position of the Raman spectrum when BSA is in solution as a reference. This research has shown that the α-helices are only still existing in a BSA solution in a coupled plasmonic nanocavities, when the neutral linking molecules are used. Using neutral linking molecules also showed that besides this α-helix, both the side groups and the β-sheets have also present in the spectrum.

Using a positively and negatively charged SAM layer, the hydrogen bond structures changes which result into disappearing of the of the signature of α-helices. In the case of the neutral and positive linking molecules, the signature of the β-sheets are more visible. In addition, the spectral signature of side chains Tyr, Phe and Trp are present in the SERS spectra. Phe and Tyr are apparent when a negative linking molecules is used, while Trp is present when a positive and neutral linking molecules are used. When Trp is detected, it may be accompanied by a weak Amide II signal. When no linking molecules are used, it is confirmed that the protein has no preference in attaching to the nanoparticles.

The signal to noise ratio is also one of the parameters that is important for detecting the BSA. In the coupled plasmonic nanocavity, the signal to noise ratio is determined by SERS enhancement that each structure is giving. We used MPA as a negatively charged, MUD as a neutral and Cys as a positively charged linking molecule. Our results show that negatively charged linking molecules give the highest intensities due to its short length (0.7 nm), followed by a positively charged linking molecule, and when no linking molecule is used. These two give almost the same intensities. Neutral linking molecules result in the lowest intensities.

Acknowledgements

I would like to thank the following people for enabling and supporting with my Bachelor thesis: my daily supervisor M.R. Aghdaee and my main supervisor dr. O.S. Ojambati. I also want to thank dr. S. Pudd. for completing the graduation committee as external supervisor and the interest in the research. In addition, I would also like to thank the other people of the Dynamic Nanophotonics group for their input. Finally, I would like to thank the other people of the NBP department for making this possible.

References

[1] K. J. Park, C. Wu, A. R. Mercer-Smith, R. A. Dodson, T. L. Moersch, P. Koonath, A. C. R. Pipino, H.-W. Lu, Y. Yang, V. S. Sapirstein, C. J. Taylor, and A. Niemz, "Raman system for sensitive and selective identification of volatile organic compounds," *Sens. Actuators, B*, vol. 220, pp. 491–499, Dec. 2015.

[2] J. Langer *et al.*, "Present and Future of Surface-Enhanced Raman Scattering," *ACS Nano*, vol. 14, pp. 28–117, Jan. 2020.

[3] L. Guerrini and R. A. Alvarez-Puebla, "Surface-Enhanced Raman Spectroscopy in Cancer Diagnosis, Prognosis and Monitoring," *Cancers*, vol. 11, June 2019.

[4] Z. Cui, L. Lu, Y. Guan, S. Ramakrishna, and M. Hong, "Enhancing SERS detection on a biocompatible metallic substrate for diabetes diagnosing," *Opt. Lett.*, vol. 46, pp. 3801–3804, Aug. 2021.

[5] X. Wang, S. Li, H. Qu, L. Hao, T. Shao, K. Wang, Z. Xia, Z. Li, and Q. Li, "SERS-based immunomagnetic bead for rapid detection of H5N1 influenza virus," *Influenza Other Respi. Viruses*, vol. 17, p. e13114, Mar. 2023.

[6] S. X. Leong, Y. X. Leong, E. X. Tan, H. Y. F. Sim, C. S. L. Koh, Y. H. Lee, C. Chong, L. S. Ng, J. R. T. Chen, D. W. C. Pang, L. B. T. Nguyen, S. K. Boong, X. Han, Y.-C. Kao, Y. H. Chua, G. C. Phan-Quang, I. Y. Phang, H. K. Lee, M. Y. Abdad, N. S. Tan, and X. Y. Ling, "Noninvasive and Point-of-Care Surface-Enhanced Raman Scattering (SERS)-Based Breathalyzer for Mass Screening of Coronavirus Disease 2019 (COVID-19) under 5 min," *ACS Nano*, vol. 16, pp. 2629–2639, Feb. 2022.

[7] A. I. Pérez-Jiménez, D. Lyu, Z. Lu, G. Liu, and B. Ren, "Surface-enhanced Raman spectroscopy: benefits, trade-offs and future developments," *Chem. Sci.*, vol. 11, pp. 4563–4577, May 2020.

[8] C. Guo, X. Guo, W. Chu, N. Jiang, and H. Li, "Spectroscopic study of conformation changes of bovine serum albumin in aqueous environment," *Chin. Chem. Lett.*, vol. 30, pp. 1302–1306, June 2019.

[9] T. Sanvictores and F. Farci, "Biochemistry, Primary Protein Structure," in *StatPearls [Internet]*, StatPearls Publishing, Oct. 2022.

[10] "Protein structure: Primary, secondary, tertiary & quatrenary (article) | Khan Academy," July 2023. [Online; accessed 6. Jul. 2023].

[11] G. P. Szekeres and J. Kneipp, "SERS Probing of Proteins in Gold Nanoparticle Agglomerates," *Front. Chem.*, vol. 7, p. 434849, Jan. 2019.

[12] H. Ma, X. Tang, Y. Liu, X. X. Han, C. He, H. Lu, and B. Zhao, "Surface-Enhanced Raman Scattering for Direct Protein Function Investigation: Controlled Immobilization and Orientation," *Anal. Chem.*, vol. 91, pp. 8767–8771, July 2019.

[13] X. X. Han, C. Köhler, J. Kozuch, U. Kuhlmann, L. Paasche, A. Sivanesan, I. M. Weidinger, and P. Hildebrandt, "Potential-Dependent Surface-Enhanced Resonance Raman Spectroscopy at Nanostructured TiO2: A Case Study on Cytochrome b5," *Small*, vol. 9, pp. 4175–4181, Dec. 2013.

[14] B. Sharma, R. R. Frontiera, A.-I. Henry, E. Ringe, and R. P. Van Duyne, "SERS: Materials, applications, and the future," *Mater. Today*, vol. 15, pp. 16–25, Jan. 2012.

[15] Y. C. Cho and S. I. Ahn, "Fabricating a Raman spectrometer using an optical pickup unit and pulsed power," *Sci. Rep.*, vol. 10, pp. 1–8, July 2020.

[16] W. Li, "Physics Models of Plasmonics: Single Nanoparticle, Complex Single Nanoparticle, Nanodimer, and Single Nanoparticle over Metallic Thin Film," *Plasmonics*, vol. 13, pp. 997–1014, June 2018.

[17] A. Agrawal, I. Kriegel, and D. J. Milliron, "Shape-Dependent Field Enhancement and Plasmon Resonance of Oxide Nanocrystals," *J. Phys. Chem. C*, vol. 119, pp. 6227–6238, Mar. 2015.

[18] Z. Wang, Z. M. Zhang, X. Quan, and P. Cheng, "A numerical study on effects of surrounding medium, material, and geometry of nanoparticles on solar absorption efficiencies," *Int. J. Heat Mass Transfer*, vol. 116, pp. 825–832, Jan. 2018.

[19] T. Chung, S.-Y. Lee, E. Y. Song, H. Chun, and B. Lee, "Plasmonic Nanostructures for Nano-Scale Bio-Sensing," *Sensors*, vol. 11, pp. 10907–10929, Nov. 2011.

[20] J. J. Baumberg, J. Aizpurua, M. H. Mikkelsen, and D. R. Smith, "Extreme nanophotonics from ultrathin metallic gaps," *Nat. Mater.*, vol. 18, pp. 668–678, July 2019.

[21] M. N. Kinalwa, E. W. Blanch, and A. J. Doig, "Accurate Determination of Protein Secondary Structure Content from Raman and Raman Optical Activity Spectra," *Anal. Chem.*, vol. 82, pp. 6347–6349, Aug. 2010.

[22] B. Jachimska and A. Pajor, "Physico-chemical characterization of bovine serum albumin in solution and as deposited on surfaces," *Bioelectrochemistry*, vol. 87, pp. 138–146, Oct. 2012.

[23] J. Grdadolnik, "Conformation of Bovine Serum Albumin as a Function of Hydration Monitored by Infrared Spectroscopy | The Infrared and Raman Discussion Group," 2002. [Online; accessed 7. Jun. 2023].

[24] S. He, M. Huang, W. Ye, D. Chen, S. He, L. Ding, Y. Yao, L. Wan, J. Xu, and S. Miao, "Conformational Change of Bovine Serum Albumin Molecules at Neutral pH in Ultra-Diluted Aqueous Solutions," *J. Phys. Chem. B*, vol. 118, pp. 12207–12214, Oct. 2014.

[25] N. Kuhar, S. Sil, and S. Umapathy, "Potential of Raman spectroscopic techniques to study proteins," *Spectrochim. Acta, Part A*, vol. 258, p. 119712, Sept. 2021.

[26] H. Fabian and W. Mäntele, "Infrared Spectroscopy of Proteins," in *Handbook of Vibrational Spectroscopy*, Chichester, England, UK: John Wiley & Sons, Ltd, Dec. 2001.

[27] N. S. Myshakina, Z. Ahmed, and S. A. Asher, "Dependence of Amide Vibrations on Hydrogen Bonding," *J. Phys. Chem. B*, vol. 112, pp. 11873–11877, Sept. 2008.

[28] J. J. Babcock and L. Brancaleon, "Bovine serum albumin oligomers in the E- and B-forms at low protein concentration and ionic strength," *Int. J. Biol. Macromol.*, vol. 53, p. 42, Feb. 2013.

[29] R. Lu, W.-W. Li, A. Katzir, Y. Raichlin, H.-Q. Yu, and B. Mizaikoff, "Probing the secondary structure of bovine serum albumin during heat-induced denaturation using mid-infrared fiberoptic sensors," *Analyst*, vol. 140, no. 3, pp. 765–770, 2015.

[30] K. Kubiak-Ossowska, B. Jachimska, and P. A. Mulheran, "How negatively charged proteins adsorb to negatively charged surfaces - a molecular dynamics study of BSA adsorption on silica," Oct. 2016. [Online; accessed 4. Jul. 2023].

[31] A. Hauptmann, G. Hoelzl, M. Mueller, K. Bechtold-Peters, and T. Loerting, "Raman Marker Bands for Secondary Structure Changes of Frozen Therapeutic Monoclonal Antibody Formulations During Thawing," *J. Pharm. Sci.*, vol. 112, pp. 51–60, Jan. 2023.

[32] A. Barth and C. Zscherp, "What vibrations tell about proteins," *Q. Rev. Biophys.*, vol. 35, pp. 369–430, Nov. 2002.

[33] S. Mangialardo, F. Piccirilli, A. Perucchi, P. Dore, and P. Postorino, "Raman analysis of insulin denaturation induced by high-pressure and thermal treatments," *J. Raman Spectrosc.*, vol. 43, pp. 692–700, June 2012.

[34] J. Kong and S. Yu, "Fourier transform infrared spectroscopic analysis of protein secondary structures," *Acta Biochim. Biophys. Sin.*, vol. 39, no. 8, pp. 549–559, 2007.

[35] K. Murayama and M. Tomida, "Heat-induced secondary structure and conformation change of bovine serum albumin investigated by Fourier transform infrared spectroscopy," *Biochemistry*, vol. 43, no. 36, pp. 11526–11532, 2004.

[36] G. Zhu, X. Zhu, Q. Fan, and X. Wan, "Raman spectra of amino acids and their aqueous solutions," *Spectrochim. Acta, Part A*, vol. 78, pp. 1187–1195, Mar. 2011.

[37] B. Hernández, F. Pflüger, S. G. Kruglik, and M. Ghomi, "Characteristic Raman lines of phenylalanine analyzed by a multiconformational approach," *J. Raman Spectrosc.*, vol. 44, pp. 827–833, June 2013.

[38] W. B. Fischer and H. H. Eysel, "Polarized Raman spectra and intensities of aromatic amino acids phenylalanine, tyrosine and tryptophan," *Spectrochim. Acta, Part A*, vol. 48, pp. 725–732, May 1992.

[39] B. Sjöberg, S. Foley, B. Cardey, and M. Enescu, "An experimental and theoretical study of the amino acid side chain Raman bands in proteins," *Spectrochim. Acta, Part A*, vol. 128, pp. 300–311, July 2014.

[40] H. T. M. Phan, S. Bartelt-Hunt, K. B. Rodenhausen, M. Schubert, and J. C. Bartz, "Investigation of Bovine Serum Albumin (BSA) Attachment onto Self-Assembled Monolayers (SAMs) Using Combinatorial Quartz Crystal Microbalance with Dissipation (QCM-D) and Spectroscopic Ellipsometry (SE)," *PLoS One*, vol. 10, no. 10, 2015.

[41] A. Faucett, "Voltage-Induced Reduction of Graphene Oxide," *Dissertation Abstracts International*, Sept. 2016.

[42] G. Yang and D. T. Hallinan, "Self-assembly of large-scale crack-free gold nanoparticle films using a 'drain-to-deposit' strategy," *Nanotechnology*, vol. 27, p. 225604, Apr. 2016.

[43] Q.-H. Guo, C.-J. Zhang, C. Wei, M.-M. Xu, Y.-X. Yuan, R.-A. Gu, and J.-L. Yao, "Controlling dynamic SERS hot spots on a monolayer film of Fe3O4@Au nanoparticles by a magnetic field," *Spectrochim. Acta, Part A*, vol. 152, pp. 336–342, Jan. 2016.

[44] K. Kim and K. S. Shin, "Surface-enhanced Raman scattering: a powerful tool for chemical identification," *Anal. Sci.*, vol. 27, no. 8, pp. 775–783, 2011.

[45] D. Radziuk and H. Moehwald, "Prospects for plasmonic hot spots in single molecule SERS towards the chemical imaging of live cells," *Phys. Chem. Chem. Phys.*, vol. 17, pp. 21072–21093, Aug. 2015.

[46] J. Dawson, "Protein Secondary Structure," Jan. 2021. [Online; accessed 6. Jul. 2023].

[47] P. P. Jing, Y. X. Li, Y. H. Su, W. L. Liang, and Y. X. Leng, "The role of metal ions in the behavior of bovine serum albumin molecules under physiological environment," *Spectrochim. Acta, Part A*, vol. 267, p. 120604, Feb. 2022.

[48] L. Xing, K. Lin, X. Zhou, S. Liu, and Y. Luo, "Multistate Mechanism of Lysozyme Denaturation through Synchronous Analysis of Raman Spectra," *J. Phys. Chem. B*, vol. 120, pp. 10660–10667, Oct. 2016.

[49] N. Kuhar, S. Sil, T. Verma, and S. Umapathy, "Challenges in application of Raman spectroscopy to biology and materials," *RSC Adv.*, vol. 8, no. 46, pp. 25888–25908, 2018.

[50] C. Kharmyssov, K. Sekerbayev, Z. Nurekeyev, A. Gaipov, and Z. N. Utegulov, "Mechano-Chemistry across Phase Transitions in Heated Albumin Protein Solutions," *Polymers*, vol. 15, p. 2039, Apr. 2023.

[51] L. Zhou, Y. Yang, H. Ren, Y. Zhao, Z. Wang, F. Wu, and Z. Xiao, "Structural Changes in Rice Bran Protein upon Different Extrusion Temperatures: A Raman Spectroscopy Study," *J. Chem.*, vol. 2016, Mar. 2016.

[52] A. Sivanesan, H. K. Ly, J. Kozuch, M. Sezer, U. Kuhlmann, A. Fischer, and I. M. Weidinger, "Functionalized Ag nanoparticles with tunable optical properties for selective protein analysis," *Chem. Commun.*, vol. 47, pp. 3553–3555, Mar. 2011.

[53] L. Cai, G. Fang, J. Tang, Q. Cheng, and X. Han, "Label-Free Surface-Enhanced Raman Spectroscopic Analysis of Proteins: Advances and Applications," *Int. J. Mol. Sci.*, vol. 23, p. 13868, Nov. 2022.

[54] L.-J. Xu, C. Zong, X.-S. Zheng, P. Hu, J.-M. Feng, and B. Ren, "Label-Free Detection of Native Proteins by Surface-Enhanced Raman Spectroscopy Using Iodide-Modified Nanoparticles," *Anal. Chem.*, vol. 86, pp. 2238–2245, Feb. 2014.

[55] J. Peters, E. Park, R. Kalyanaraman, A. Luczak, and V. Ganesh, "Protein Secondary Structure Determination Using Drop Coat Deposition Confocal Raman Spectroscopy," *Spectroscopy*, vol. 31, pp. 31–39, Oct. 2016.

[56] P. Candeloro, E. Grande, R. Raimondo, D. Di Mascolo, F. Gentile, M. L. Coluccio, G. Perozziello, N. Malara, M. Francardi, and E. Di Fabrizio, "Raman database of amino acids solutions: a critical study of Extended Multiplicative Signal Correction," *Analyst*, vol. 138, pp. 7331–7340, Nov. 2013.

A Appendix: Supporting information

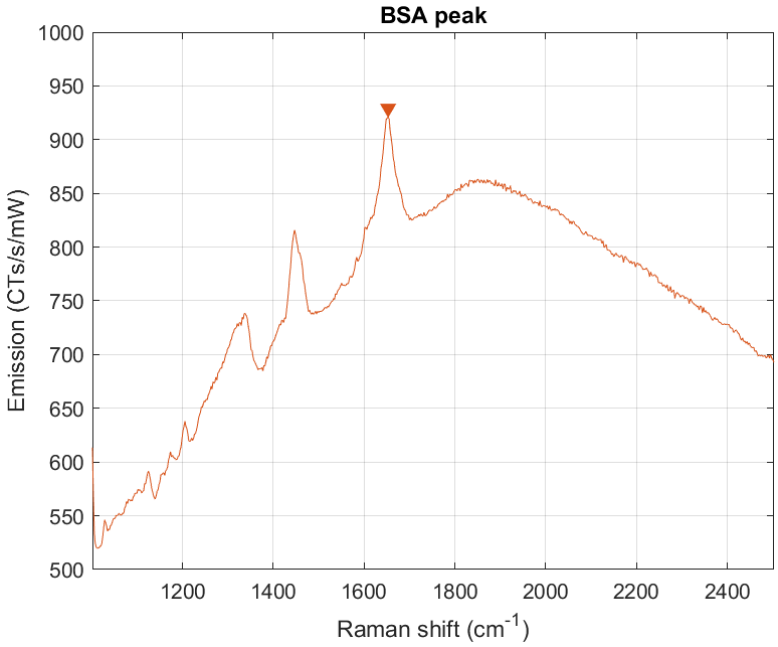

Figure 21: This graphs shows the BSA emission in the solution. The Raman shift peak of this measurement is around 1653 cm^{-1}. This is a previously made measurement made by the department. The data is provided by the supervisor.

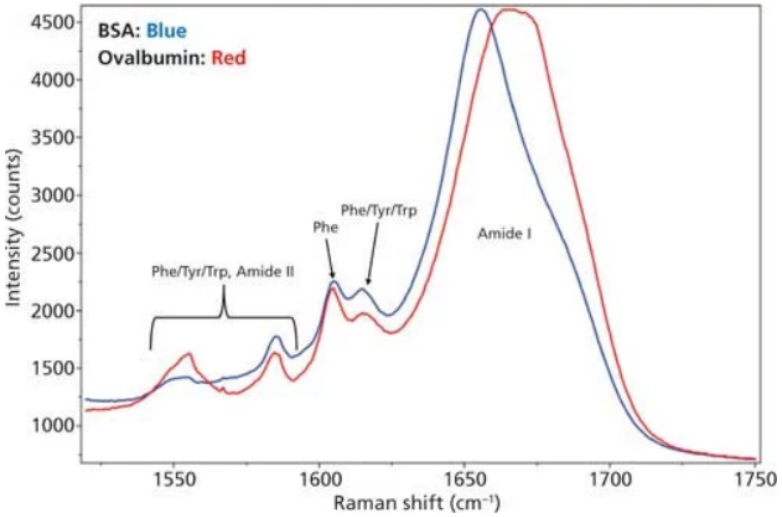

Figure 22: This spectrum shows the Raman shift peaks of Amide I and the side groups of BSA.(55)

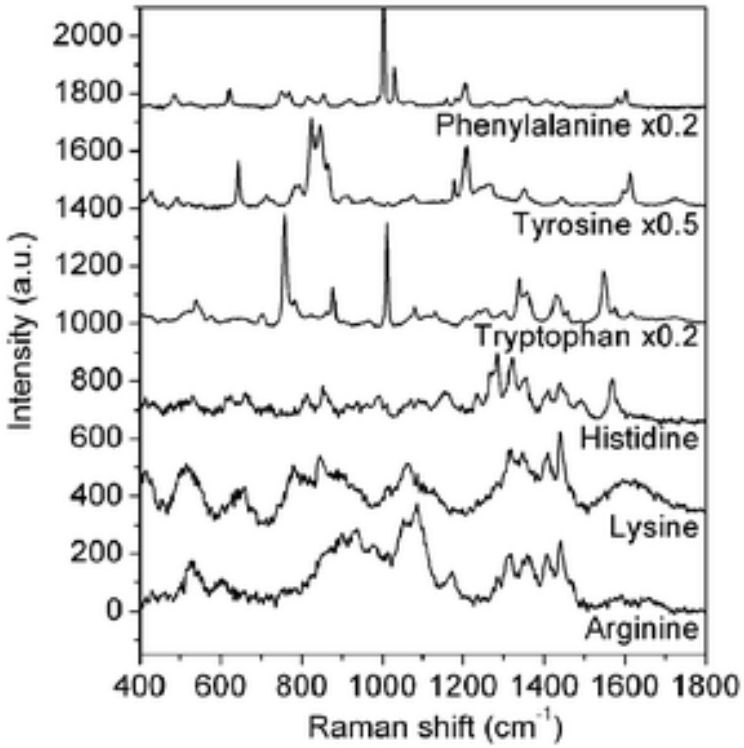

Figure 23: This spectra show the Raman shift peaks of the side groups of BSA.(56)

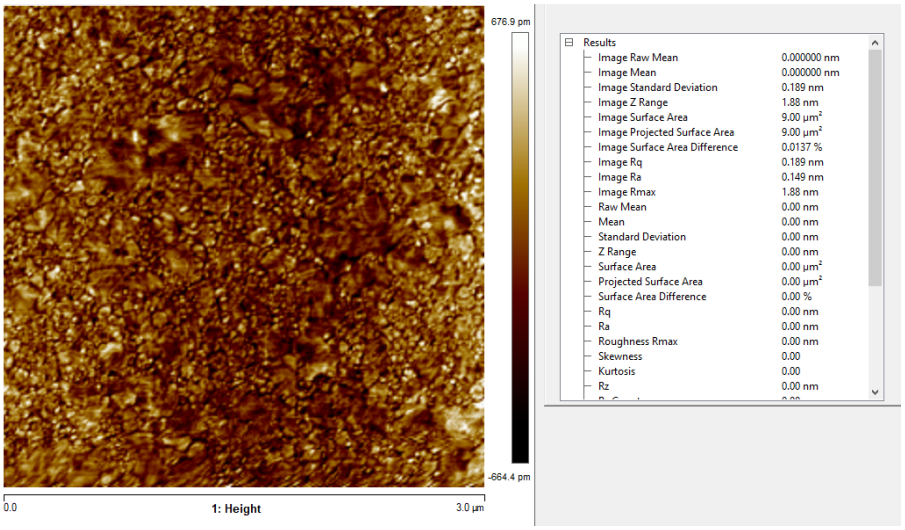

Figure 24: This AFM image with the resulting values shows that the surface is really smooth.

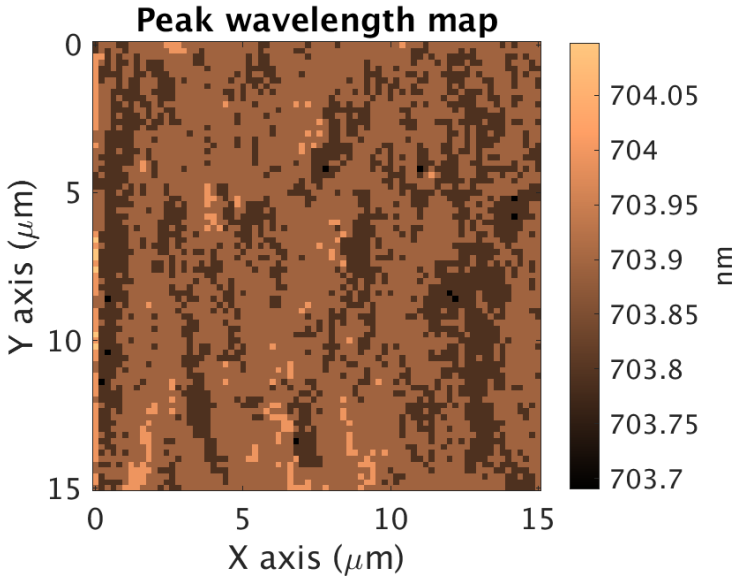

Figure 25: This peak wavelength map shows that there is only a really small Raman shift if the small molecule methylene blue is used.

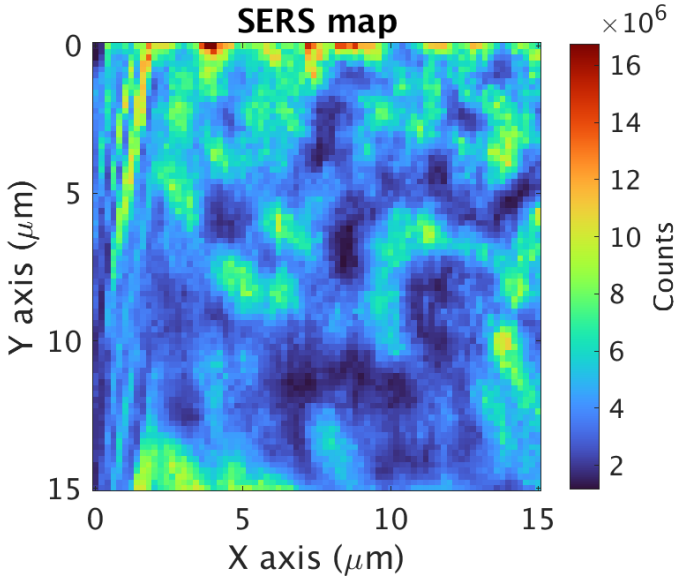

Figure 26: This SERS intensity map shows that there are intensity fluctuations, even if the small molecule methylene blue is used.

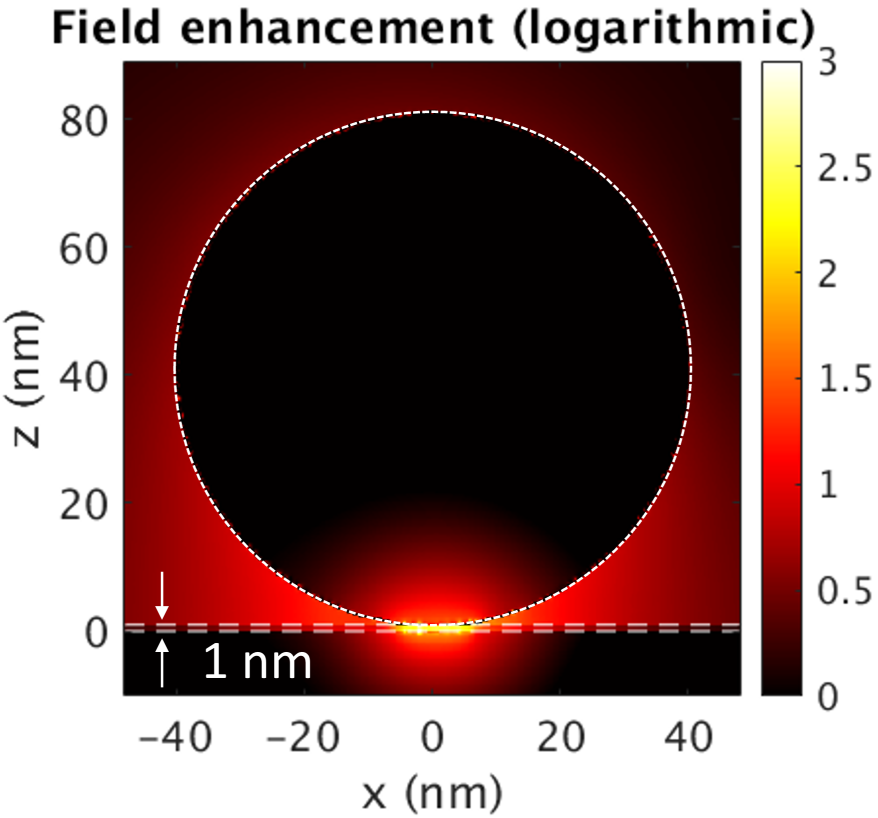

Figure 27: This shows that the greatest field enhancement is within a few nanometers from the hotspot. This image is provided by the supervisor.

B Appendix: Protocols chemical lab

B.1 Protocol for fabricating gold aggregation

This protocol is used for making gold nanoparticles aggregation on top of the gold thin layer.

1. Clean the tweezers and work with green gloves
   Clean it with aceton, demi-water and ethanol respectively. Dry it with nitrogen.

2. Take the chambers
   Stick the chambers with tape, stick the tube with tape and check the black carbon tape whether it is well attached and it is still sticky.

3. Pick up one thin layer, put it in the chamber and then in the fume hood
   Cut it out and place the glassy side on the bottom. Put plastic on the chamber to prevent dust.

4. Prepare the substances

   (a) 1 mL hexane (Sigma: 650552)

   (b) a mix of 0.5 mL butylamine (Sigma: 471305, diluted to 1 mM with demi-water) and 0.5 mL ethanol (Supelco: 1.00983)

(c) a mix of 1.0 mL gold nanoparticles and 1.0 mL ethanol (Supelco: 1.00983)
Shake the nanoparticles vial well before using. After mixing it with ethanol, centrifuge it for 4-5 minutes so that the nanoparticles have settled to the bottom. You will see a red line nanoparticles. Rotate it a few times till all the nanoparticles are in the bottom. Take out 1 mL of the mix. Do not aspirate the nanoparticles, so make sure you only take out the transparent part. Then you have 1 mL left. Mix it with the pipetboy.

5. Make the mix
First put the 1 mL gold nanoparticles + ethanol in the chamber on the gold thin layer. Then put 1 mL butylamine + ethanol in the chamber and lastly put 1 mL hexane in the chamber. Mix all the components gently with the pipetboy, with a maximum of two times. Wait at least two hours.

6. Pump the liquid out of the chamber
Use a pump with a rate of 0.1 mL/min and diameter of 14.5 mm. Make sure the *Withdraw* LED is on. Connect the tube of the chamber to the syringe. After pumping out the liquid, let the sample dry for around half an hour. Place the sample in a petri dish and save it in the nitrogen box.

B.2 Protocol for soaking linking molecules and proteins

This protocol is used for soaking the linking molecules and the proteins. If you do not want to use the linking molecule, skip step 1 and 2.

1. Let soak the linking molecules
Put the gold thin layer in a small sample jar with the glassy side on the bottom. Add 0.5 mL linking molecules to it. Let is soak for 24 hours.

2. Take out the linking molecules
After 24 hours, pick the gold thin layer with a tweezers. Rinse it with ethanol and dry it with nitrogen.

3. Let soak the protein
Put the gold thin layer in a small sample jar with the glassy side on the bottom. Add 1.0 mL protein to it. Let is soak for 24 hours.

4. Take out the protein
After 24 hours, pick the gold thin layer with a tweezers. Do not rinse it. Dry the sample with nitrogen.

B.3 Protocol for making new solutions

This protocol is used for making new solutions. For powders, the *Mass Molarity Calculator* of *Sigma-Aldrich* can be used, which applies the following equation to calculate the required mass:

$$Mass\ (g) = Concentration\ (mol/L) \cdot Volume\ (L) \cdot Molecular\ weight\ (g/mol) \tag{1}$$

- BSA (Sigma: A7906-100G)
Solvent: milli-Q water
How to mix it: first fill the tube with milli-Q water, then add the BSA powder. Let it mix for one day and then try to shake it gently so that the proteins do not break down.

- Cysteamine hydrochloride (Sigma: 49705)
  Solvent: ethanol (Supelco: 1.00983)
  How to mix it: first fill the tube with ethanol (Supelco: 1.00983), then add the powder. Shake to mix it.

- MUD (Sigma: 447528)
  Solvent: ethanol (Supelco: 1.00983)
  How to mix it: first fill the tube with ethanol (Supelco: 1.00983), then add the powder. Shake to mix it.

For liquids, the *Solution Dilution Calculator* of *Sigma-Aldrich* can be used, which applies the following equations to calculate the desired concentration:

$$Mass_1 \cdot Volume_1 = Mass_2 \cdot Volume_2 \tag{2}$$

$$Stock\ concentration\ (mM) = \frac{Density\ (g/mL)}{Molecular\ weight\ (g/mol)} * 10^6 \tag{3}$$

- MPA (Sigma: M5801-5G)
  Solvent: (Supelco: 1.00983)
  How to mix it: shake it

- Butylamine (Sigma: 471305) in two steps
  Solvent: milli-Q water
  How to mix it: first make a new stock, by diluting it to a concentration of 100 mM. After that, dilute it again to the desired concentration. Shake to mix it.

Other liquids that do not need to be diluted:

- Hexane (Sigma: 650552): got it from the PCF department in Meander, via Nathalie Schilderink
- Ethanol (Supelco: 1.00983)
- Gold nanoparticles (BBI: EM.GC80)

B.4 Protocol for template stripping

This protocol describes the produces of template stripping.

- Wash the glass covers
  1. Clean the jar and the tweezers with ethanol
  2. Fill the jar with 50 mL ethanol
  3. Put the glass covers in the jar. Do it gently, so they do not break.
  4. Put the jar in the sonicator for 15 minutes
  5. Take out the ethanol and fill the jar with milli-Q water to rinse the glass covers and to dilute the remaining ethanol. Rinse it twice if necessary.
  6. Take out the water and fill the jar with aceton
  7. Put the jar in the sonicator for 10 minutes

8. Take out the aceton. Fill the jar with aceton again. Now the glass coves are clean.

- Implement the glass covers

1. Pick up the glass covers one by one with a tweezers
2. Dry the glass cover with nitrogen. It has to be completely dry!
3. Place the glass cover on a dust-free tissue
4. Put one little drop UV glue on the film without touching the surface
5. Place the glass cover on the glue and twist it gently, so the glue will distribute
6. Cure the glue with UV light

C Appendix: Protocols optical lab

C.1 Setup

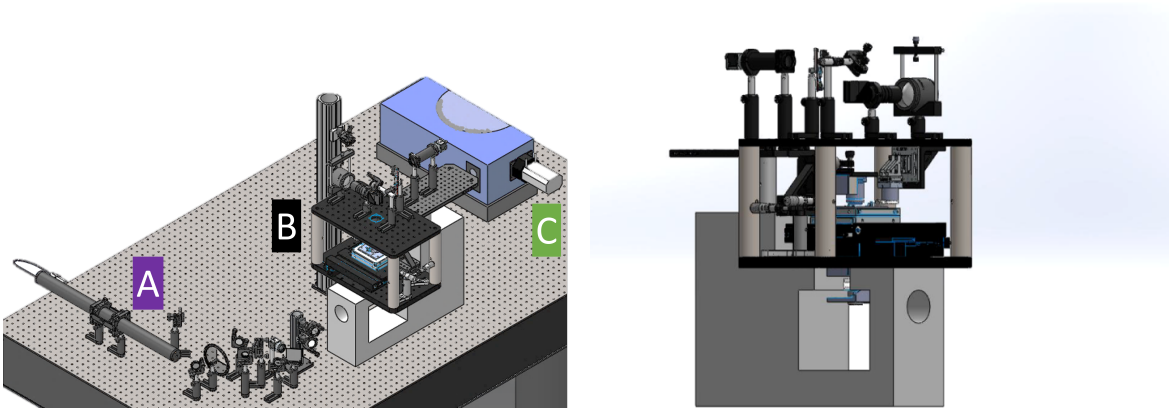

Figure 28: Left gives a representation of what the setup looks like. The setup consists of (A) an excitation source, (B) a microscope and (C) a spectroscope. The microscopy part (B) is also shown on the right.

C.2 Initializing the software

- Turn on the devices

1. Turn on the laser with the key
2. Turn on the devices with the physical buttons on it
3. Turn on the devices with the remote control (two top buttons!)
4. Turn on the spectroscope
5. Run Setup_GUI.m to open the software

- Make sure the alignment is good

1. The laser beam must follow the right path. Follow the laser beam till the objective, and then the reflective laser beam till the spectroscope. Some mirrors could not be positioned properly, or the ND filters could be closed.
2. Do a power measurement. Make sure only the laser shutter is open and the white light shutter is closed. Note the value.
3. Take an image of the laser. It must be in the center.
4. Check the position of the laser sport in the camera. It must be in the center and it has to be symmetrical when you change the z-height.

C.3 Explore the surface

- Set the z-height and focus it
  1. Open the laser shutter and close the white light shutter
  2. Set the color camera exposure time low; around 10,000 μs
  3. Turn down the z-height gently, till the laser spot becomes smaller
  4. Set the color camera exposure time very low; around 100 μs
  5. Turn down the z-height gently, till the laser spot is on its smallest
- If it is focused
  1. Close the laser shutter and open the white light shutter
  2. Set the camera exposure time back to 100,000 μs. You could increase this value a little bit.
  3. Fine-tune the z-height till the aggregation can be seen clearly. Now darkfield images and/or the Raman spectra can be made.

C.4 Make darkfield images and Raman spectra

- Make darkfield images
  Choose tab *Camera*
  Choose color camera, define saving names and choose a saving path and format
- Make Raman spectra
  Choose tab *Spectroscopy*
  Click on initialize experiment
  Choose the file *CW laser top coupling 633nm_2023_43_25* as ND
  Define saving names and choose a saving path
  Central wavelength: 720 nm
  Exposure time: 3000 ms
- Do a background measurement as reference (experiment type: background). Then do some single SERS measurements (experiment type: SERS, experiment technique: single scan, choose the reference you made). To check if there is a good signal. Finally, start a surface SERS measurement (experiment type: SERS, experiment technique: XYZ scan, choose the reference you made).

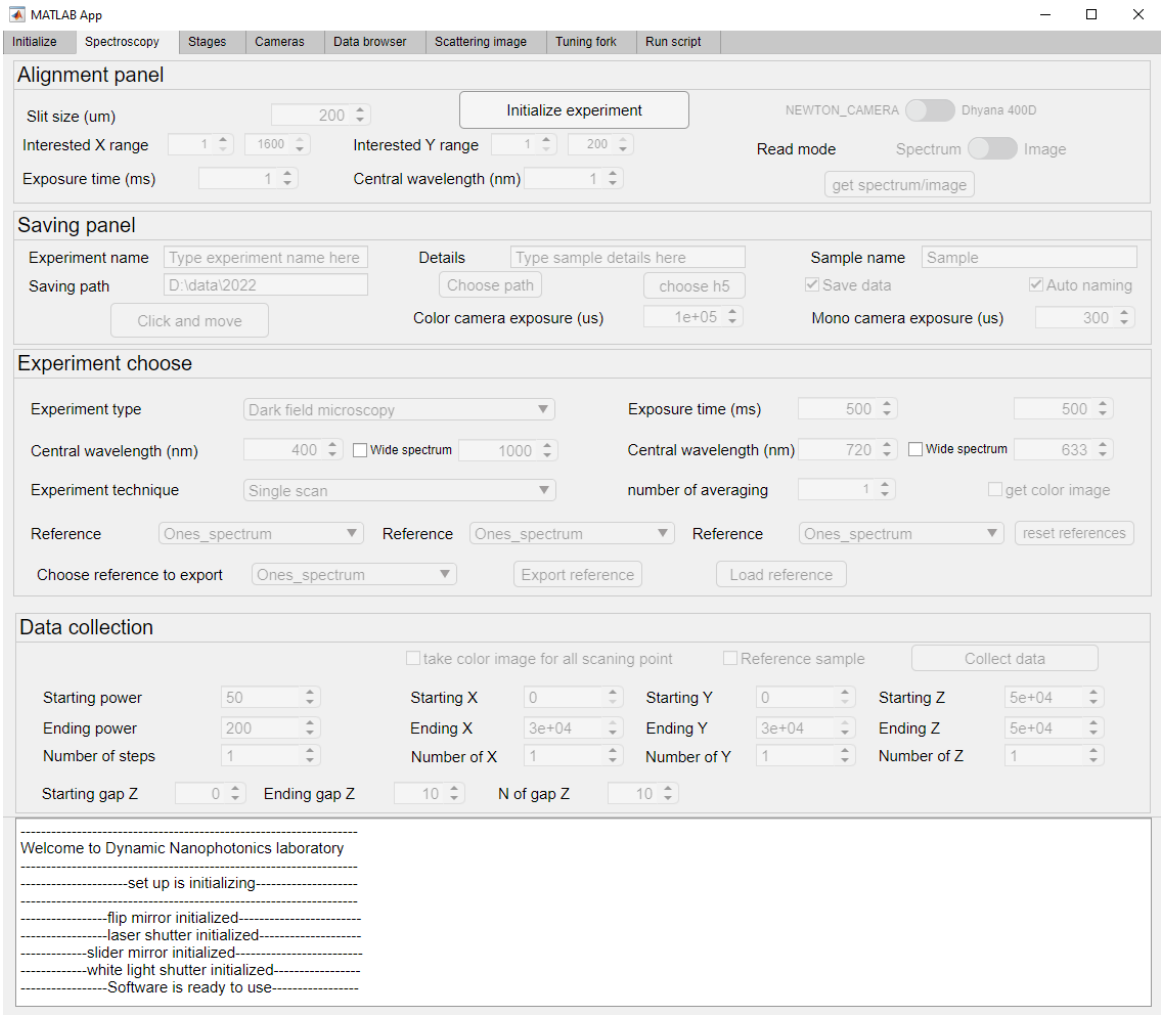

Figure 29: The software. The spectroscopy tab is shown here.

D Appendix: Results

Here all results are presented, without further analysis. One of the Raman spectra is shown, to show whether or not there is a BSA signature. A darkfield image of the scanned surface is shown. In addition, both the intensity of the most intense peak (with the condition that the minimum height is 100 $counts/(mWs)$), with the corresponding Raman shift, are shown in a 2D map with all (x,y) locations.

Open hotspot with MPA

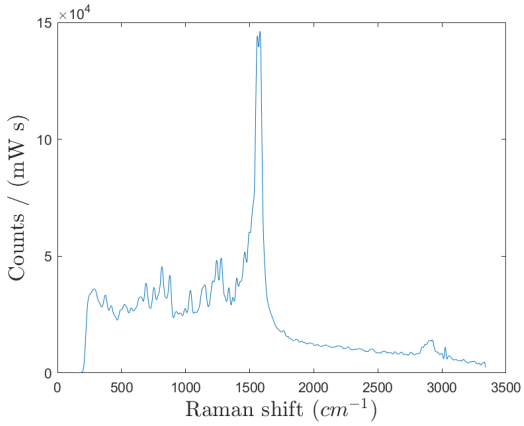

(a) BSA signature

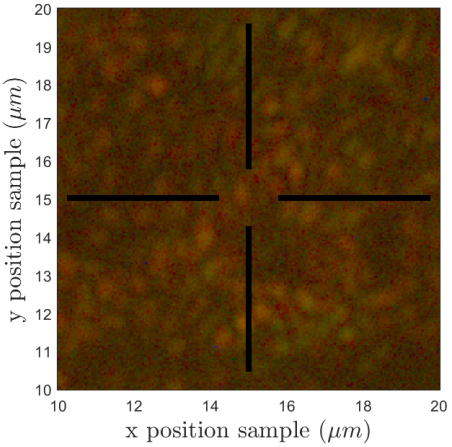

(b) Darkfield image

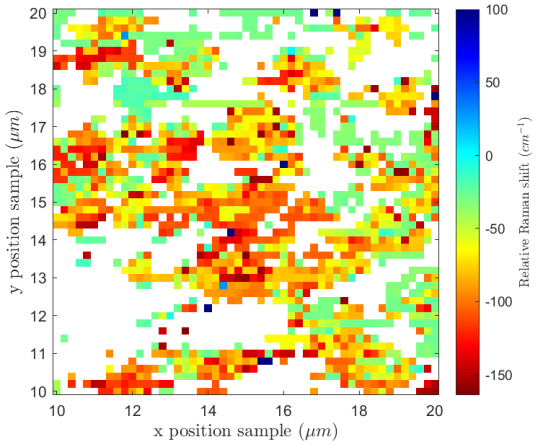

(c) Relative Raman shift

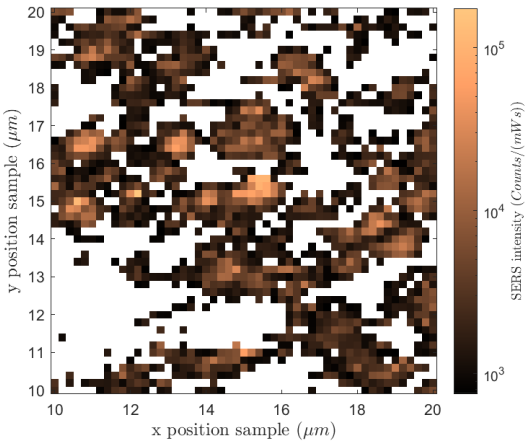

(d) SERS intensity

Figure 30: Scan 1.1 Open hotspot with MPA

Open hotspot with MPA

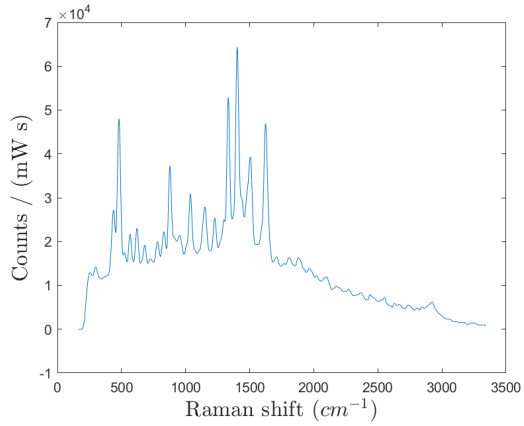

(a) BSA signature

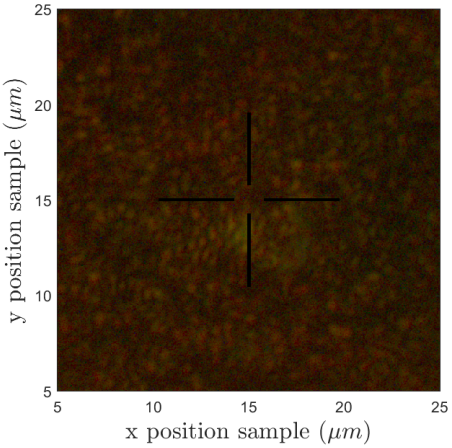

(b) Darkfield image

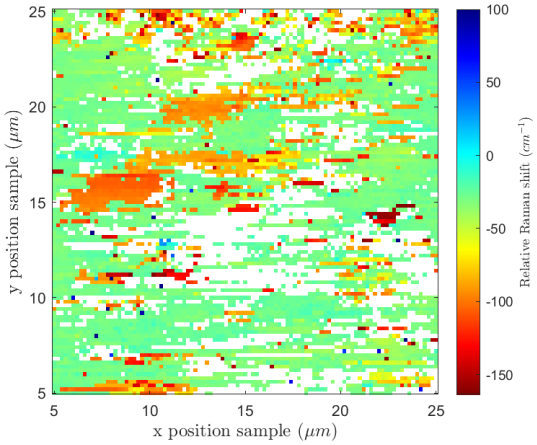

(c) Relative Raman shift

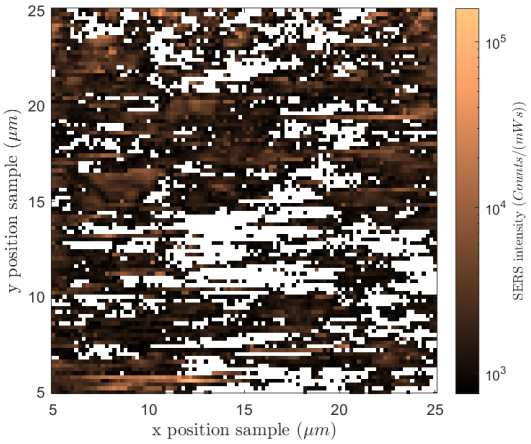

(d) SERS intensity

Figure 31: Scan 1.2 Open hotspot with MPA

Open hotspot with MPA

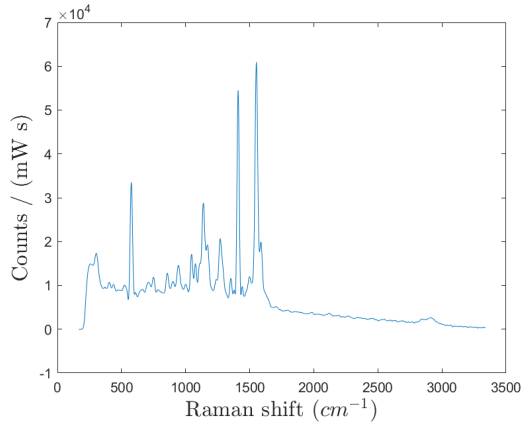

(a) BSA signature

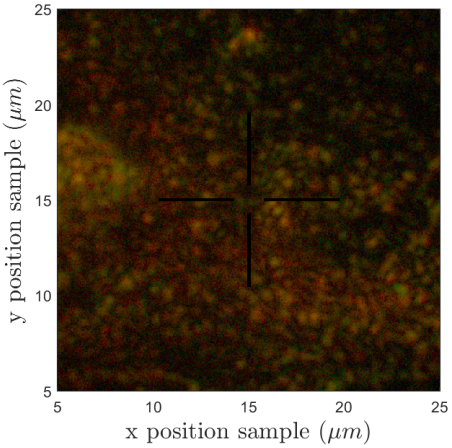

(b) Darkfield image

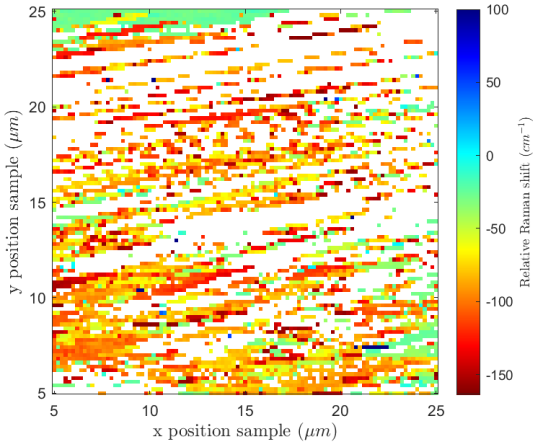

(c) Relative Raman shift

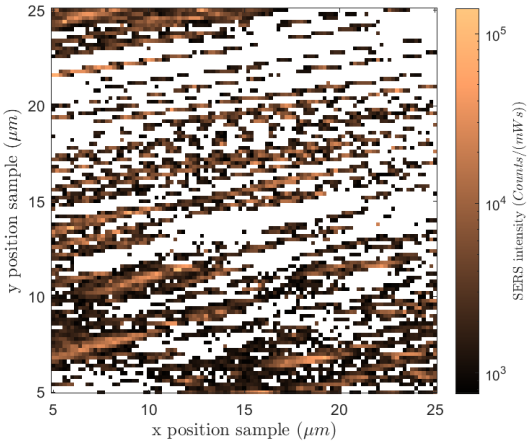

(d) SERS intensity

Figure 32: Scan 1.3 Open hotspot with MPA

Open hotspot with MPA

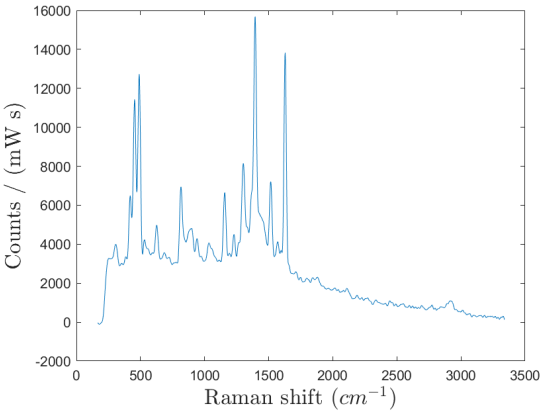

(a) BSA signature

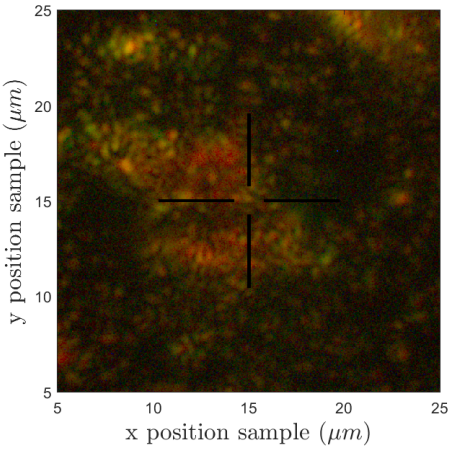

(b) Darkfield image

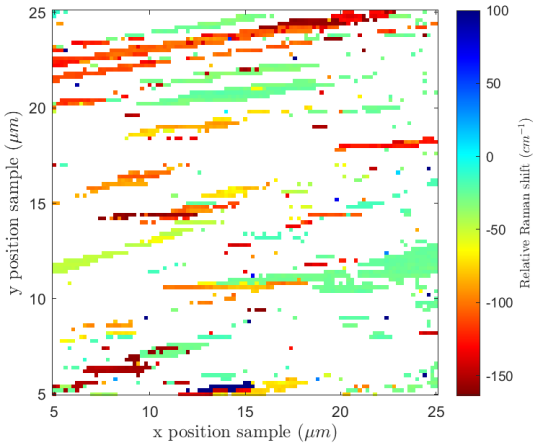

(c) Relative Raman shift

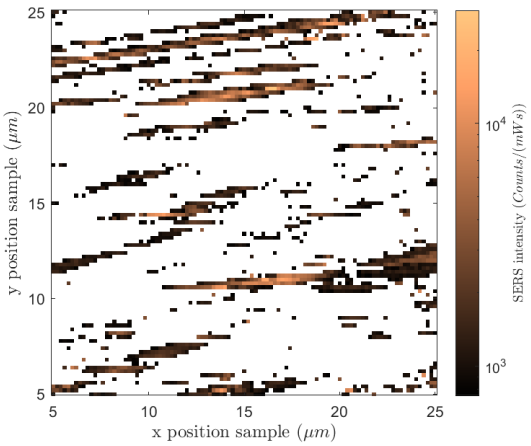

(d) SERS intensity

Figure 33: Scan 1.4 Open hotspot with MPA

Open hotspot with MPA

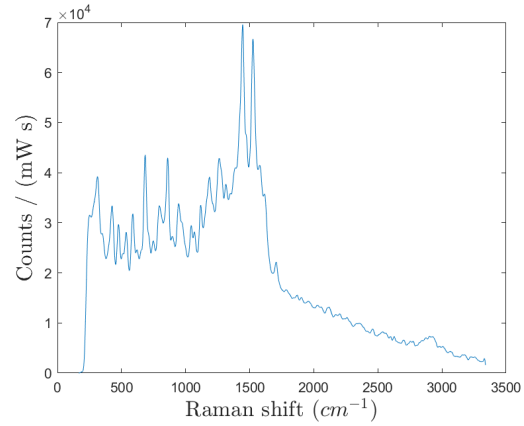

(a) BSA signature

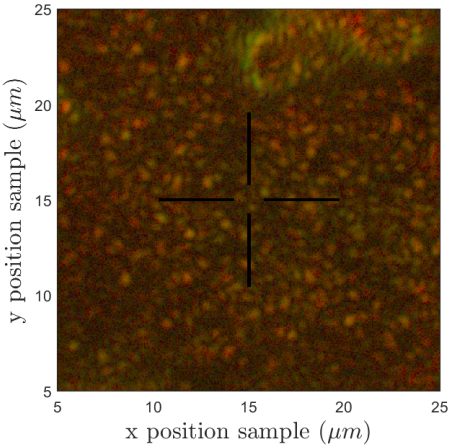

(b) Darkfield image

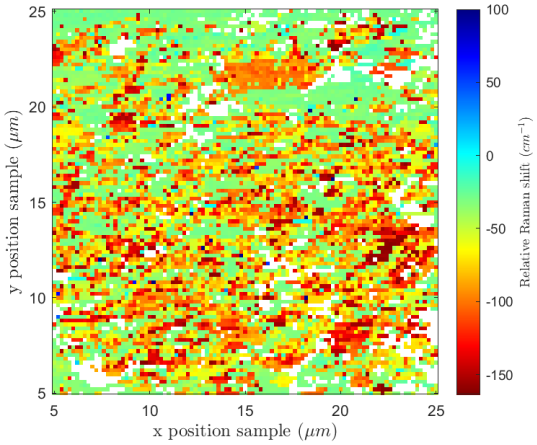

(c) Relative Raman shift

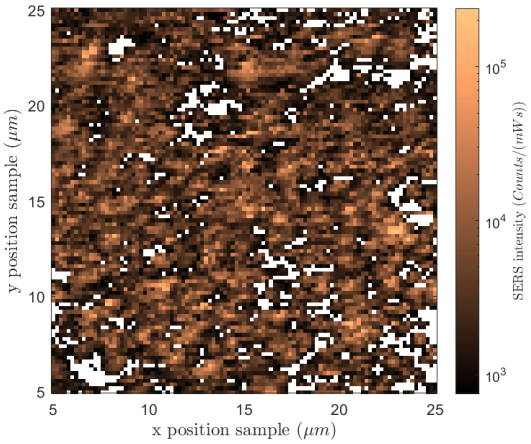

(d) SERS intensity

Figure 34: Scan 1.5 Open hotspot with MPA

Closed hotspot without any linking molecules

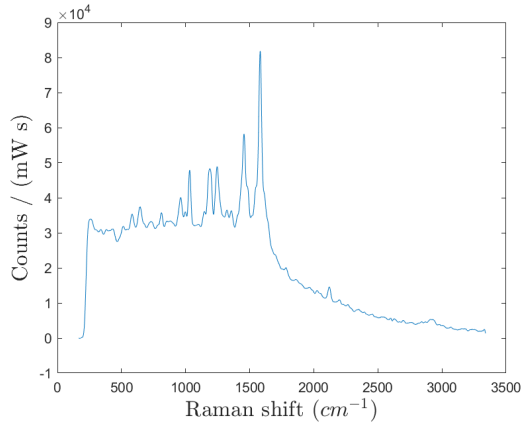

(a) BSA signature

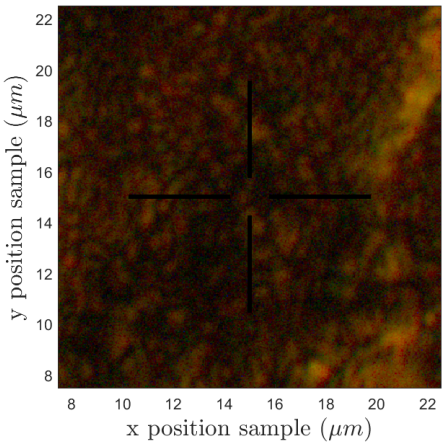

(b) Darkfield image

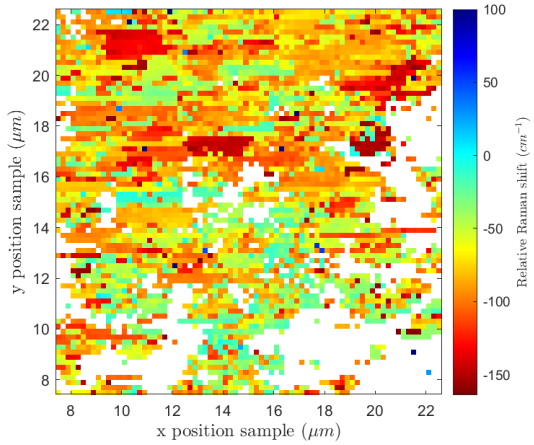

(c) Relative Raman shift

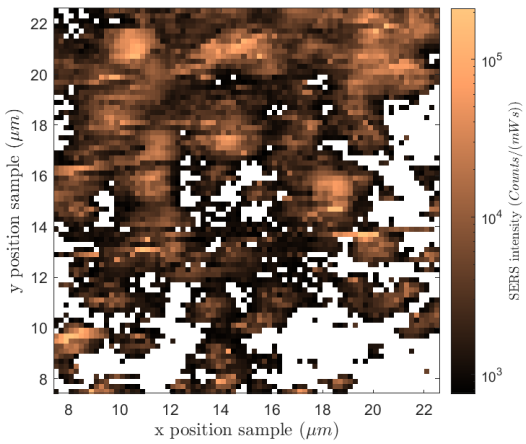

(d) SERS intensity

Figure 35: Scan 2.1 Closed hotspot without any linking molecules

Closed hotspot without any linking molecules

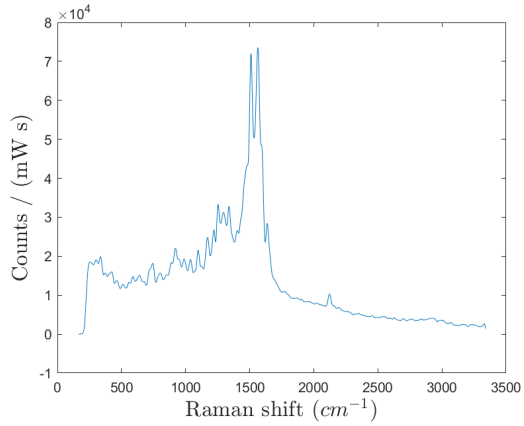

(a) BSA signature

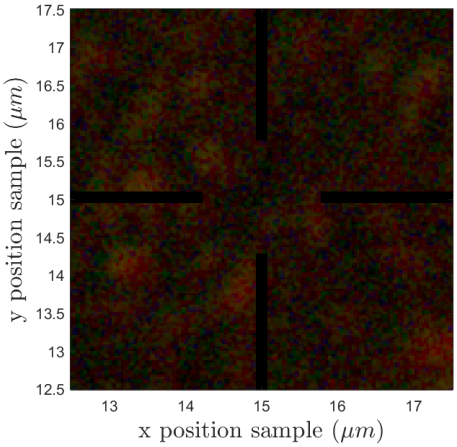

(b) Darkfield image

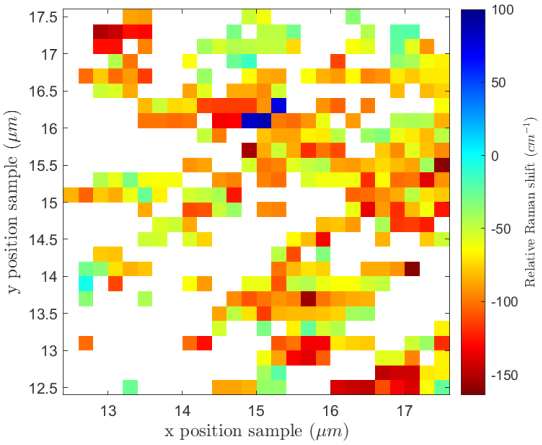

(c) Relative Raman shift

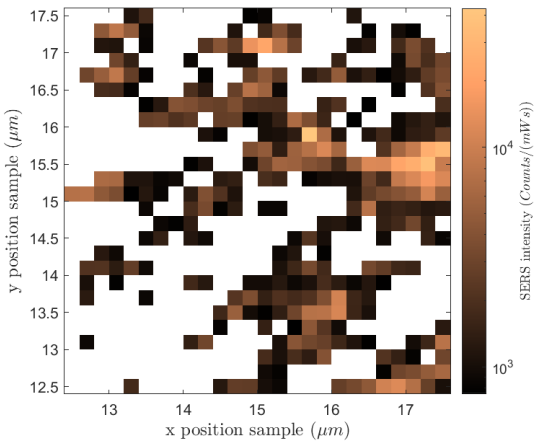

(d) SERS intensity

Figure 36: Scan 2.2 Closed hotspot without any linking molecules

Closed hotspot without any linking molecules

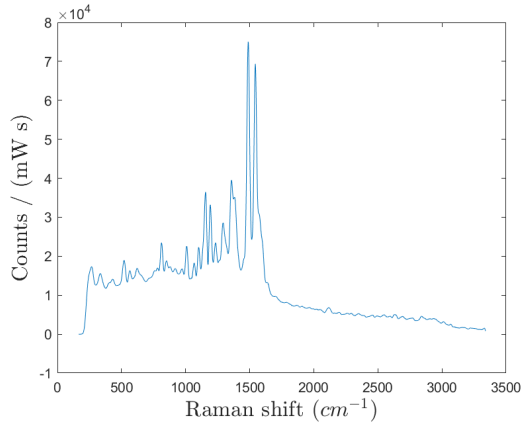

(a) BSA signature

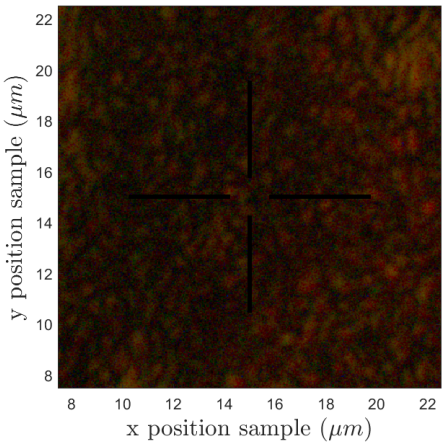

(b) Darkfield image

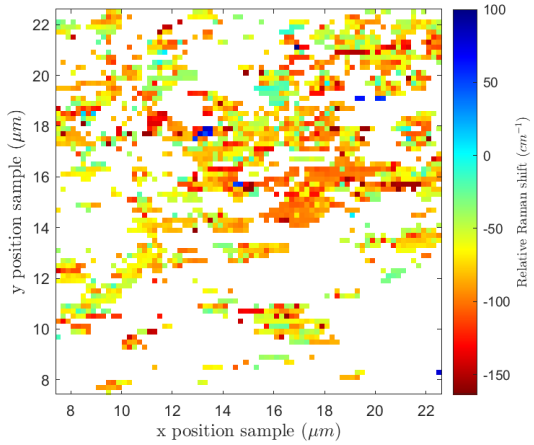

(c) Relative Raman shift

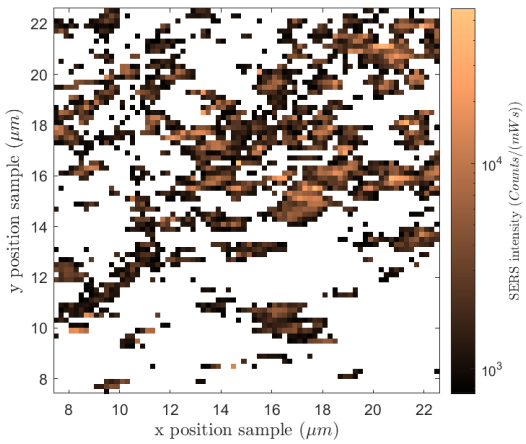

(d) SERS intensity

Figure 37: Scan 2.3 Closed hotspot without any linking molecules

Closed hotspot without any linking molecules

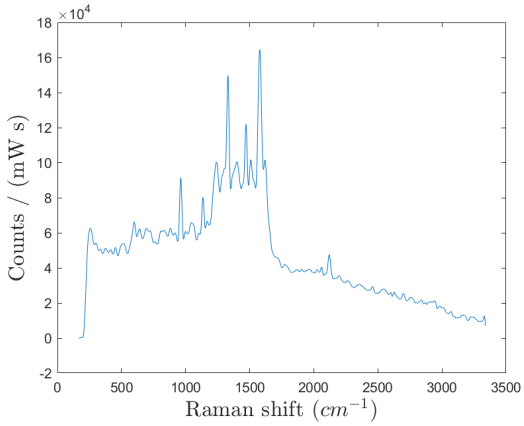

(a) BSA signature

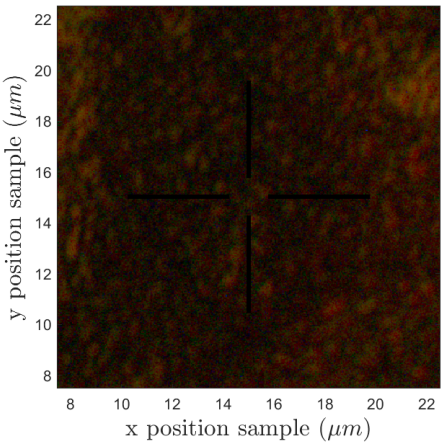

(b) Darkfield image

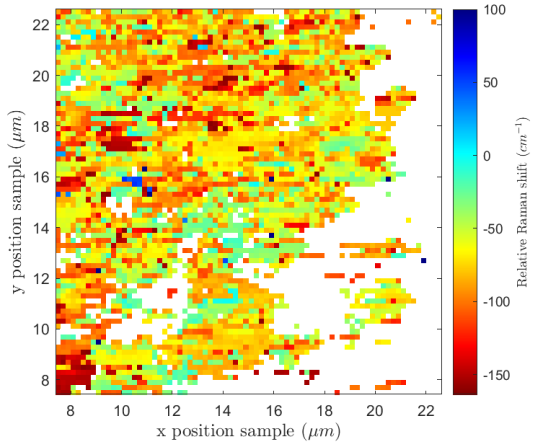

(c) Relative Raman shift

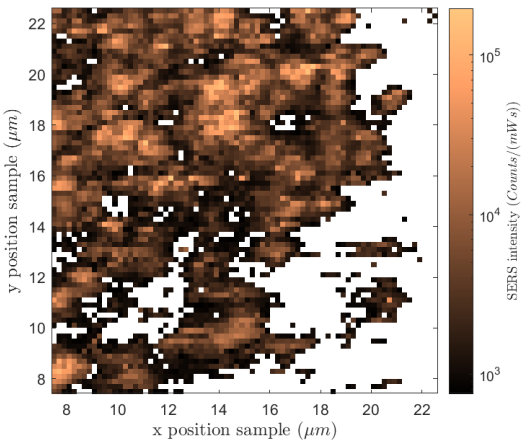

(d) SERS intensity

Figure 38: Scan 2.4 Closed hotspot without any linking molecules

Closed hotspot without any linking molecules

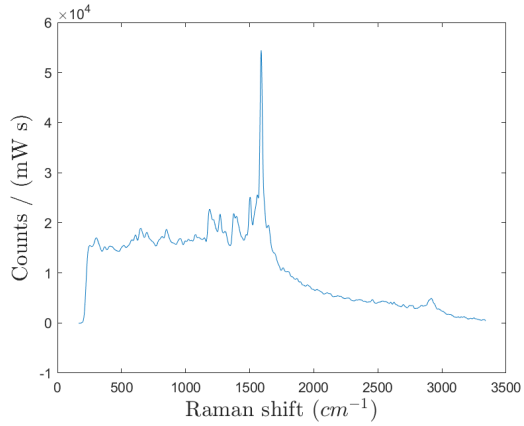

(a) BSA signature

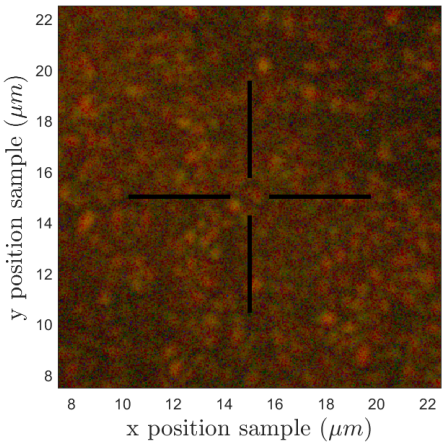

(b) Darkfield image

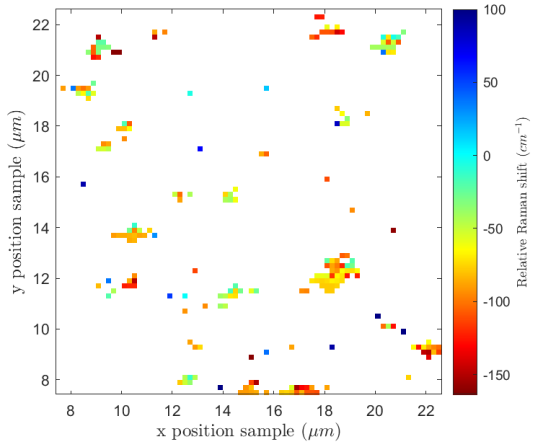

(c) Relative Raman shift

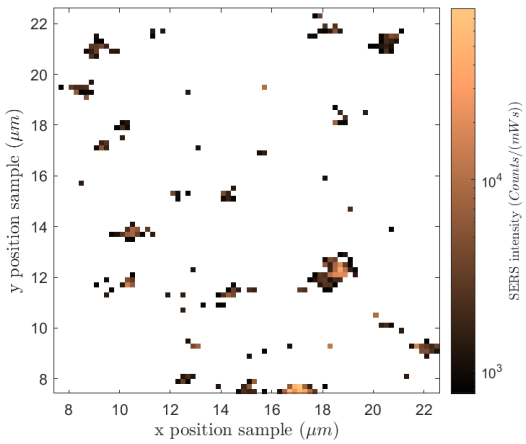

(d) SERS intensity

Figure 39: Scan 2.5 Closed hotspot without any linking molecules

Closed hotspot without any linking molecules

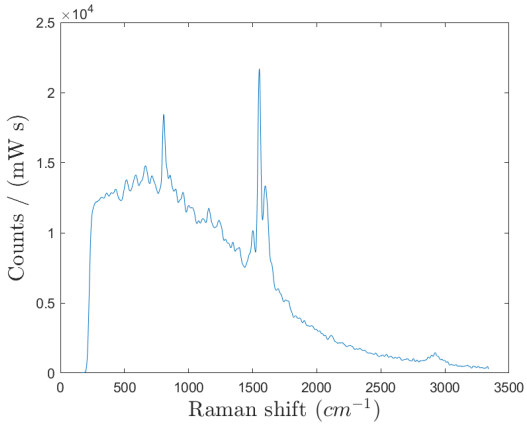

(a) BSA signature

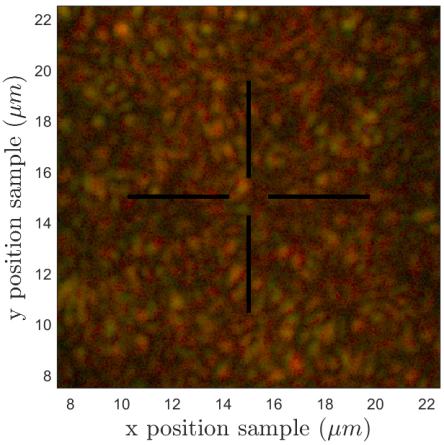

(b) Darkfield image

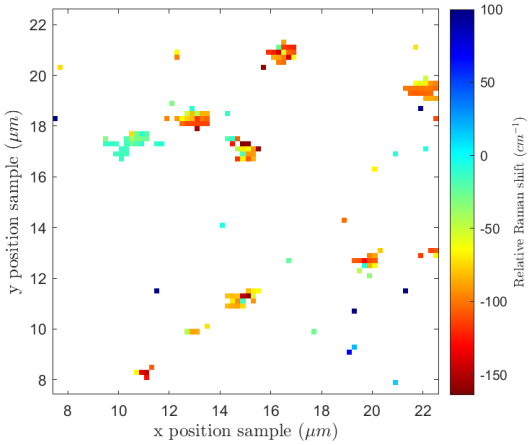

(c) Relative Raman shift

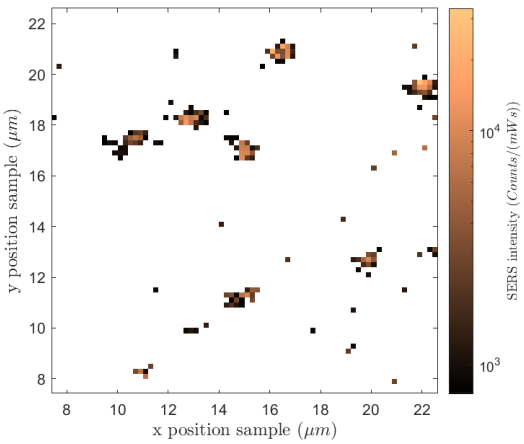

(d) SERS intensity

Figure 40: Scan 2.6 Closed hotspot without any linking molecules

Closed hotspot with Cys

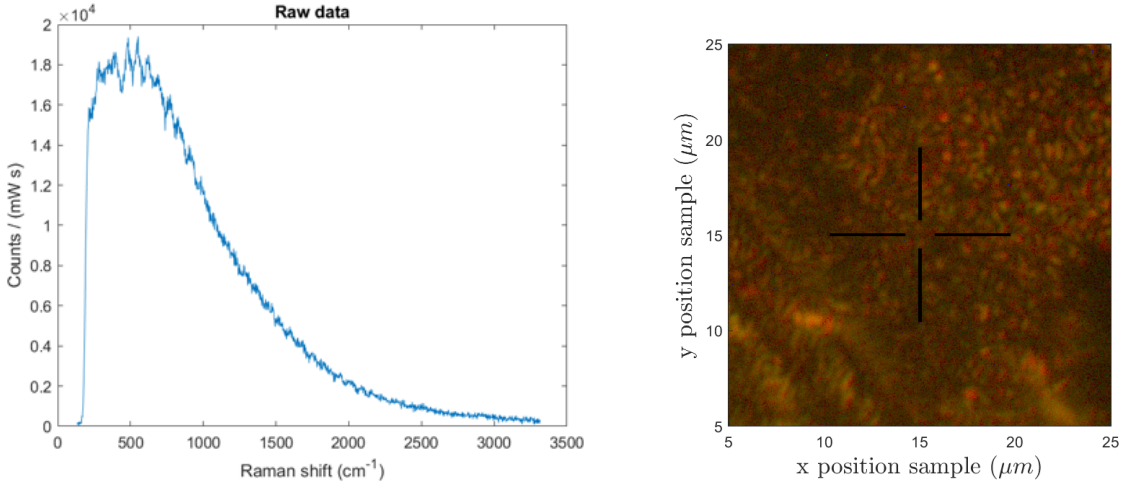

(a) BSA signature

(b) Darkfield image

Figure 41: Scan 3.1 Closed hotspot with Cys

Open hotspot with Cys

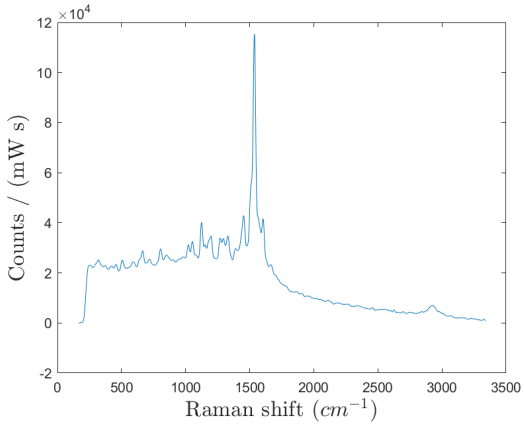

(a) BSA signature

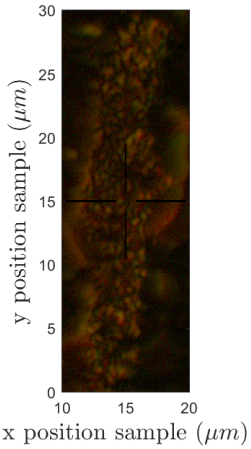

(b) Darkfield image

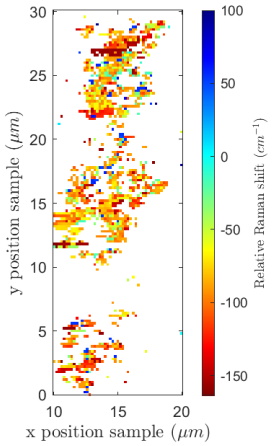

(c) Relative Raman shift

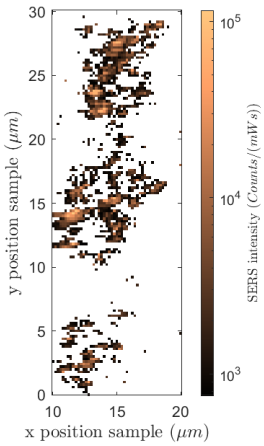

(d) SERS intensity

Figure 42: Scan 4.1 Open hotspot with Cys

Open hotspot with Cys

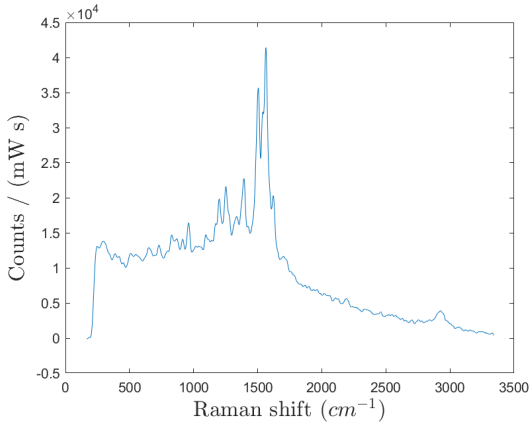

(a) BSA signature

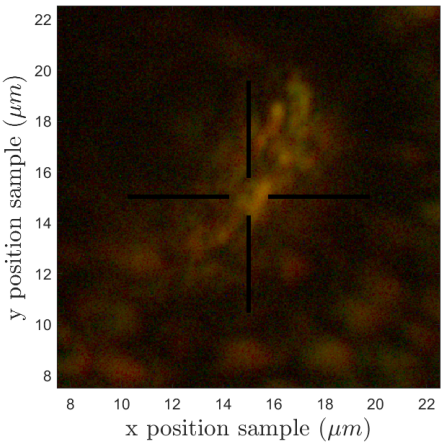

(b) Darkfield image

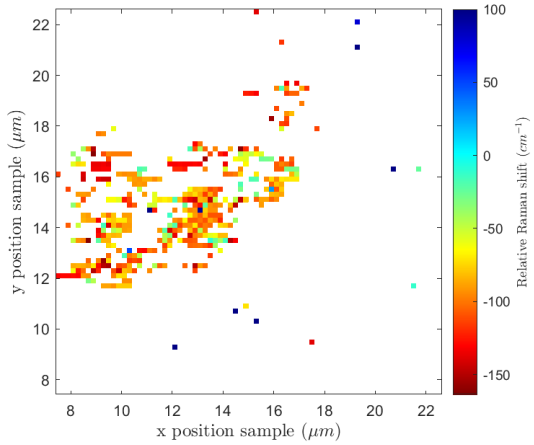

(c) Relative Raman shift

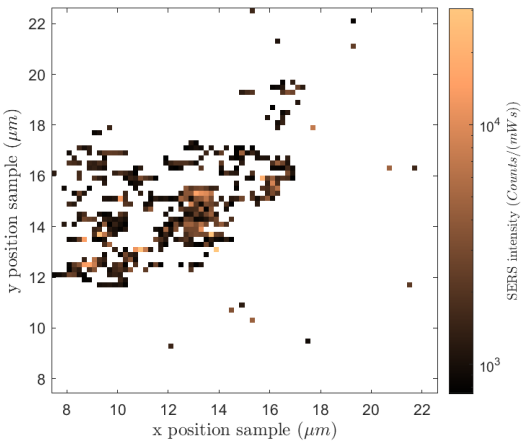

(d) SERS intensity

Figure 43: Scan 4.2 Open hotspot with Cys

Open hotspot without any linking molecules

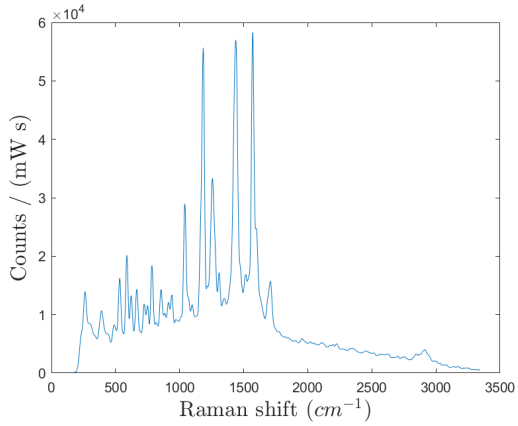

(a) BSA signature

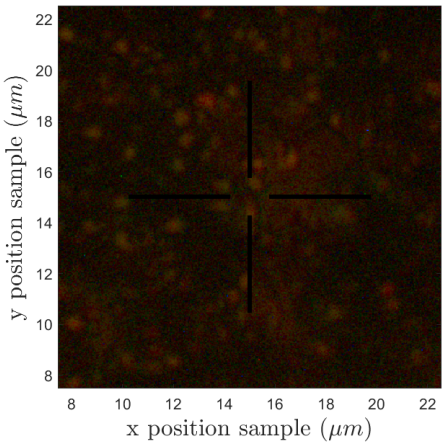

(b) Darkfield image

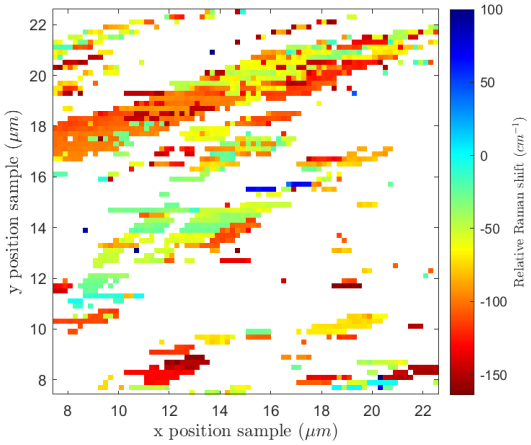

(c) Relative Raman shift

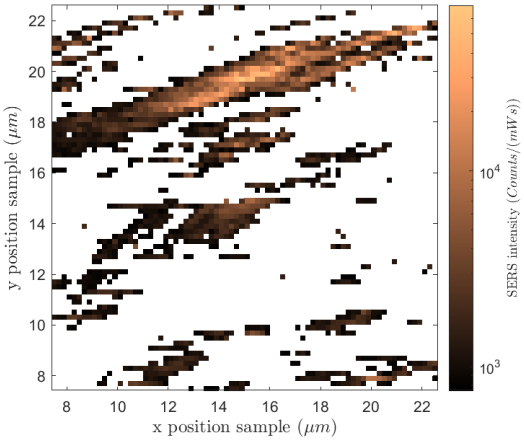

(d) SERS intensity

Figure 44: San 5.1 Open hotspot without any linking molecules

Open hotspot without any linking molecules

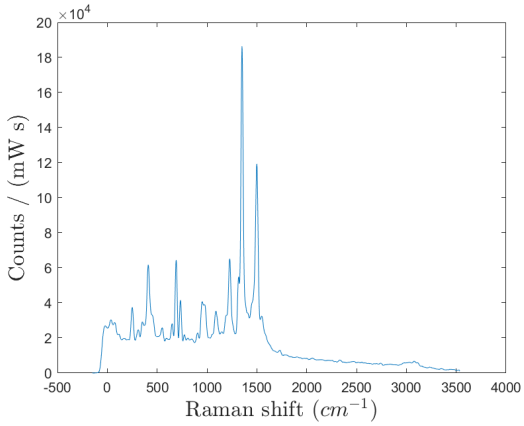

(a) BSA signature

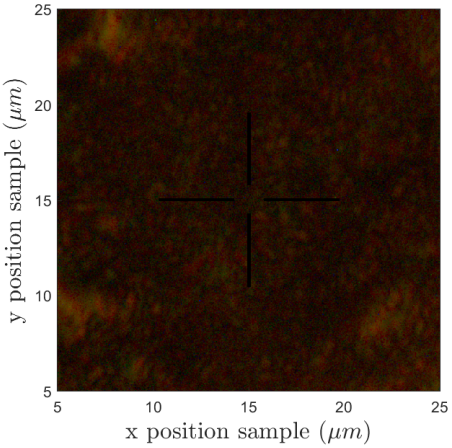

(b) Darkfield image

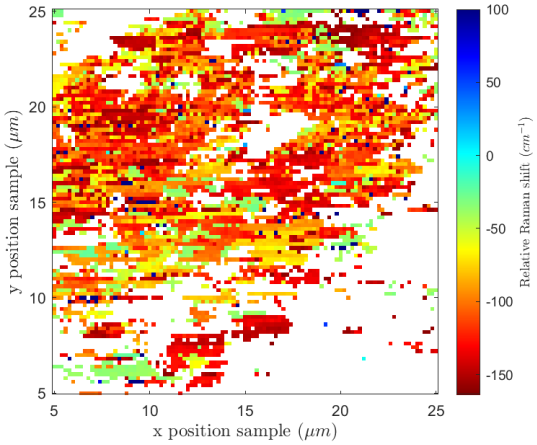

(c) Relative Raman shift

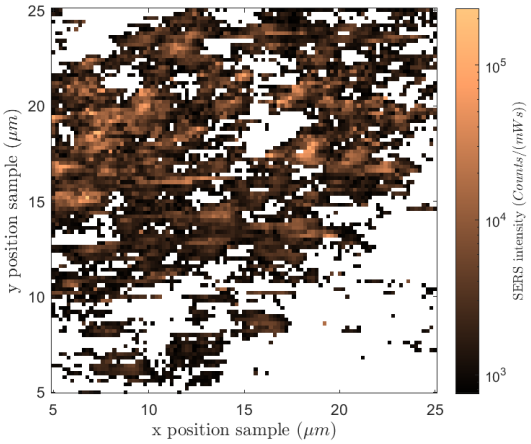

(d) SERS intensity

Figure 45: Scan 5.2 Open hotspot without any linking molecules

Open hotspot with MUD

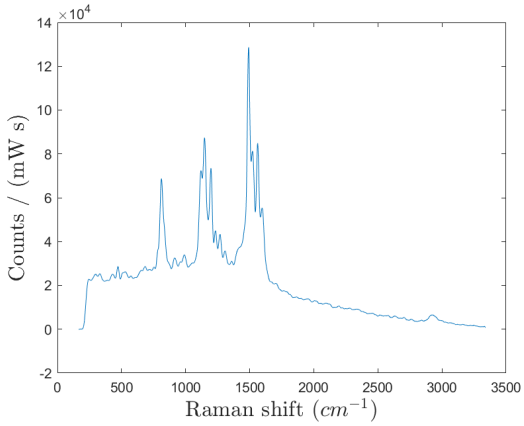

(a) BSA signature

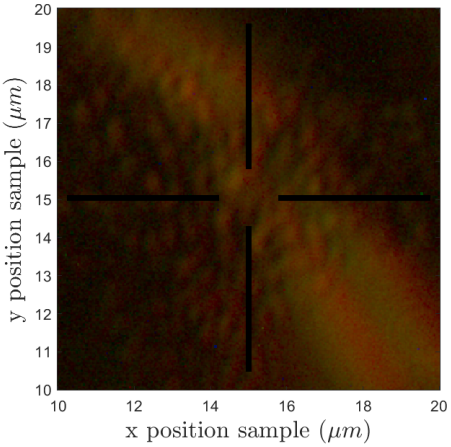

(b) Darkfield image

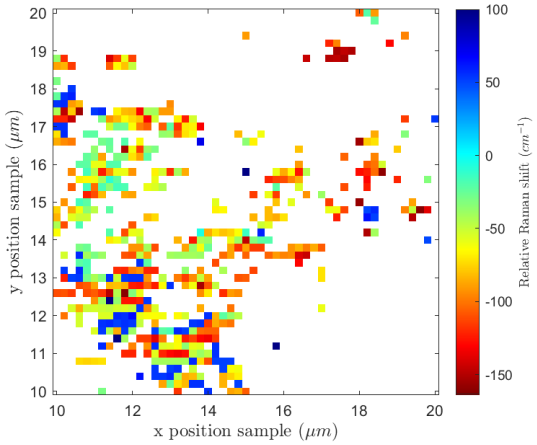

(c) Relative Raman shift

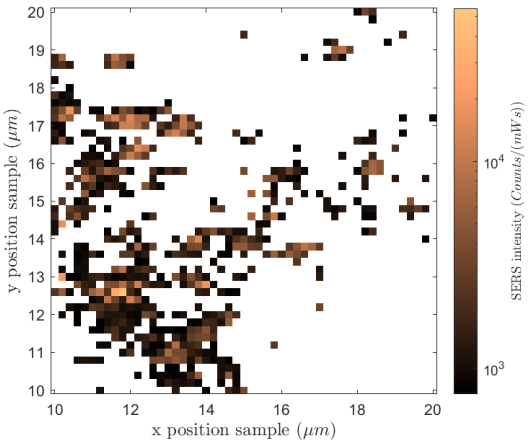

(d) SERS intensity

Figure 46: Scan 6.1 Open hotspot with MUD

Open hotspot with MUD

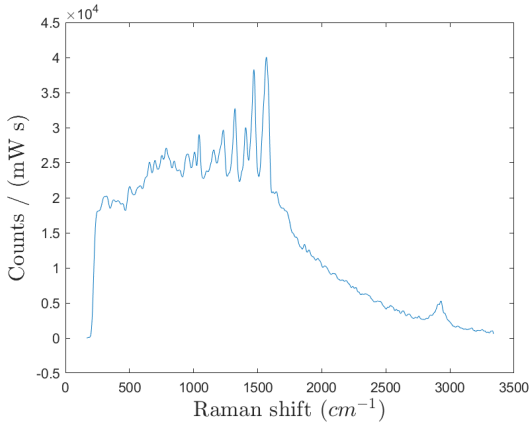

(a) BSA signature

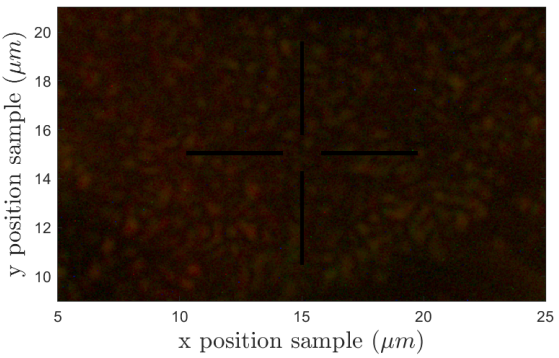

(b) Darkfield image

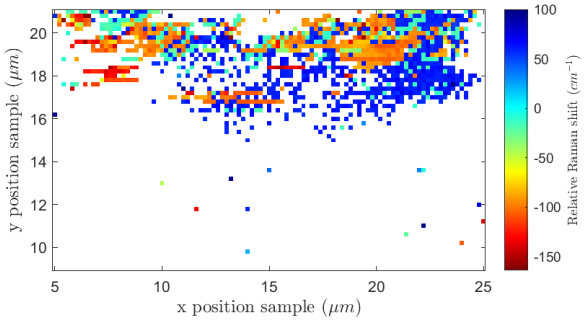

(c) Relative Raman shift

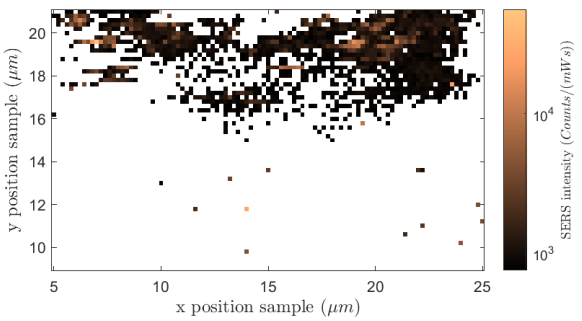

(d) SERS intensity

Figure 47: Scan 6.2 Open hotspot with MUD